An artificial CPG inspired by a pond snail

Shanmei Liu

Department of Computer Science, Memorial University

Jan. 24, 2018

Contents

Abstract

A Central Pattern Generator (CPG) is a kind of neural network capable of generating rhythmic patterned outputs. Biological CPGs regulate rhythmic motor behaviors such as breathing, feeding, swimming, and digesting, in a particularly efficient way for animals in nature. Similar mechanisms and patterns are studied and extended by researchers in mathematics and physics, and widely applied in control systems such as robotics. In this study, we explore the electrophysiological fundamentals of action potential generation and the Hodgkin-Huxley mechanism of voltage-gated ion channels. An artificial CPG represented by a system of ordinary differential equations (ODEs) was built to replicate the behavior of the respiratory CPG of a pond snail, *Lymnaea stagnalis*. The Morris-Lecar model was chosen as the starting point to represent each of the neurons in the 3-neuron network of the *Lymnaea stagnalis* CPG. This model balances the complexity and compliance of the system, and demonstrates the feasibility of modelling CPG neural networks with limited experimental data using existing neuron models. Delay was introduced into the ODE system, and the resulting artificial CPG approaches the output patterns of the original CPG better than in the ODE system. In this way, delay is shown to be effective for providing better control of timing, as well as richer behaviors in neural networks.

Introduction

Neuron excitability and Hodgkin-Huxley mechanism

Neurons are a type of cell distinguished from other cells by their unique complex shapes, particularly, the massive extensive branches. A neuron can generally be decomposed into 3 parts: cell body (soma), axon and dendrites. Dendrites are treelike thin appendages at one end of the cell (neuron); they receive impulses from other neurons and transmit electrical stimuli to the soma. The axon is a single elongated fiber that carries the nerve signal (impulse) away to other neurons. The electrical activity passing through the axon is called the **action potential,** sometimes also referred to as nerve **impulse** or **spike**, which is a rapid rise and fall in membrane potential. The soma contains the nucleus and other structures that exist in other common living cells. The most important role of the soma is producing chemicals called neurotransmitters. Neurotransmitters are chemical messengers that either excite or inhibit neighboring cells by binding to receptors at the synapse.

Synapses play the essential role in neural connectivity. They function as intermedia between the axon of the presynaptic cell, and the postsynaptic receptors. A synapse is actually a small gap (i.e. there is no physical continuity between these pre- and postsynaptic elements) at the end of a neuron that allows information to pass from one neuron to the next through the process of synaptic transmission. Most synapses connect axons to dendrites, but other types of connections also exist, including axon to-soma, axon-to-axon, and dendrite-to-dendrite. There are two types of synapses, chemical synapses and electrical synapses, which differ from each other in terms of the chemical and electrical processes in the synaptic contacts. For electrical synapses, ionic currents flow from one cell to another directly; while chemical synapses function by releasing vesicles, tiny membrane-bound spheres that contain neurotransmitters, which produce a functional change in the properties of the target cell . A chemical synapse is either inhibitory or excitability; the inhibitory effect reduces the likelihood of firing an action potential while excitatory effect increases the likelihood. A neuron may receive a large number of inhibitory and excitatory inputs at the same time, and after a complicated procedure of signal summation and processing, both the intrinsic properties and the inputs received will determine the output signal.

All living cells have a thin plasma membrane separating the intracellular components from the extracellular environment. The cell membrane is a phospholipid bilayer with embedded proteins, permeable to water molecules and a few other small, uncharged, molecules like oxygen (O_2) and carbon dioxide (CO_2). The consequence of this ion-selective permeability is that there exists a voltage difference across the membrane resulting from the difference in concentrations inside and outside the. This is the fundamental mechanism that endows cells the ability to use membrane potential for signaling by control of ionic transport.

Cells can be divided into 2 groups, excitable and non-excitable. "Excitable" means that if the applied current is strong enough, the membrane potential generates an action potential which either responds in full to a stimulus or not at all. This is the well-known all-or-none, or threshold, phenomenon as seen in most neurons. As a result, background noise is filtered out and signal can be transmitted reliably. On the other hand, non-excitable cells do not generate action potentials, their membrane potential does not change appreciably over time. All body cells except for neurons, muscle cells, and some endocrine cells are non-excitable.

The most influential work done by Alan Hodgkin and Andrew Huxley, explained how voltage-gated ion channels give rise to propagating action potentials by the quantitative description of electrical excitability in nerve cells as a set of differential equations, and revealed the mechanism of action potential generation both mathematically and biologically (Schwiening, 2012). The fundamental of Hodgkin-Huxley model (Hodgkin & Huxley, 1952) is to treat the membrane as a circuit, then reconstruct the action potential by building equations for the ion channels as shown in Figure 1. By Kirchoff's law, we have

$$C_M \frac{dV}{dt} + I_{ion} + I_L = I_{ext} \tag{1}$$

where

$$I_{ion} = \sum_k I_k = \sum_k G_k(V - E_k) \tag{2}$$

is a combination of voltage-gated ion currents, G_k denotes the conductance describing the voltage and time dependence of ionic currents such as calcium, potassium and sodium channels, usually

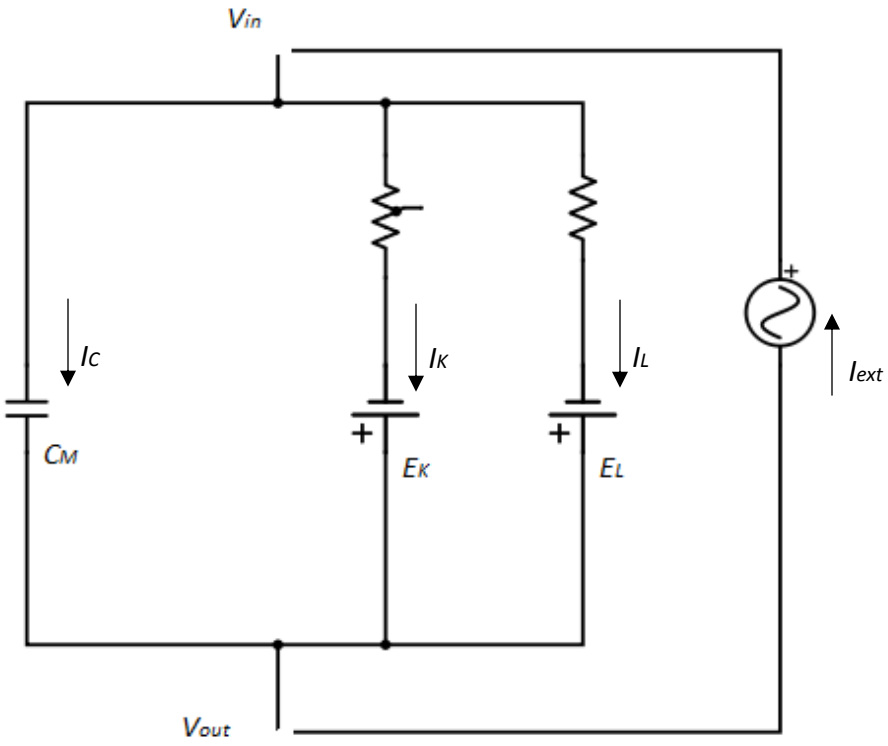

Figure 1, An electrical circuit resembles the cell membrane. The current which charges a capacitor is equal to the capacitance times the rate of change of the voltage across the capacitor.

not constant, but a function of gating variables representing the degree to which channels are opened or closed, V is the membrane potential, and E_k is the reversal potential for each channel. The leak current I_L represents the passive properties of the cell, where the conductance g_L is a constant, and I_{ext} is the external stimulus which can be an artificial injected current or synaptic input. C_M denotes the capacitance of the cell membrane.

The original model developed by Hodgkin and Huxley for the squid giant axon formulates three ion currents: sodium, potassium and leakage as described below

$$C_M \frac{dV}{dt} + g_{Na} m^3 h(V - E_{Na}) + g_K n^4 (V - E_K) + g_L (V - E_L) = I_{app} \quad (3)$$

$$\frac{dx}{dt} = -\frac{1}{\tau_x(u)}[x - x_\infty(u)], x \in m, h, n \quad (4)$$

m, h and n are dimensionless gating variables, each approaches the target value $x_\infty(u)$ with a time constant $\tau_x(u)$ for a fixed voltage value u. By setting the voltage step in the voltage clamp experiments and fitting data to the equations, the time dependence and equilibrium value of the conductance can be determined, and the non-linear equations can be reduced to the form

$$x(t) = x_\infty(u_1) - [x_\infty(u_0) - x_\infty(u_1)] e^{\frac{-(t-t_0)}{\tau_x(u_1)}} \quad (5)$$

Gating variable m is called the activation variable of the sodium channel, and h is the inactivation variable since the sodium channel is controlled by three activation gates and one inactivation gate. The potassium channel only contains four activation gates, therefore the activation variable n appears as n to the power of four. For the voltage-dependent ion channels, an activation gate means that the corresponding conductance increases with depolarization (V increases), while the inactivation gate means that the conductance decreases with depolarization (Gerstner, Kistler, Naud, & Paninski, 2014).

The dynamics of each ion channel can be described by its individual gate being in one of two states, permissive or non-permissive; for a certain gate's probability of being in the permissive state, assumed to be p, the transitions between permissive and non-permissive states can be described using the first-order kinetics (Eq. 6),

$$\frac{dp}{dt} = \alpha(1-p) + \beta p \tag{6}$$

where $\alpha(V)$ and $\beta(V)$ are voltage-dependent rate constants describing the transition rate from the permissive to the non-permissive state and non-permissive to permissive respectively. Therefore, a generalized formulation of gating variable m, h and n is given as

$$\frac{dx}{dt} = \alpha_x(1-x) + \beta_x x, x \in m, n, h \tag{7}$$

$\alpha(V)$ and $\beta(V)$ are determined by experimental measurement and can be generalized as the form:

$$\frac{A(V-B)}{e^{\left(\frac{V-B}{C}\right)} - D} \tag{8}$$

where A, B, C and D are constants fit to voltage clamp data, and V is the cell membrane potential. In Hodgkin Huxley model, the rate constants are calculated from experimental observations and given as

$$\alpha_m = \frac{0.1(25-V)}{e^{\left(\frac{25-V}{10}\right)} - 1} \tag{9}$$

$$\beta_m = 0.07e^{\left(-\frac{V}{20}\right)} \tag{10}$$

$$\alpha_n = \frac{0.01(10-V)}{e^{\frac{10-V}{10}} - 1} \tag{11}$$

$$\beta_n = 0.125e^{\left(-\frac{V}{80}\right)} \tag{12}$$

$$\alpha_h = 0.07e^{\left(-\frac{V}{20}\right)} \tag{13}$$

$$\beta_h = \frac{1}{e^{\left(\frac{30-V}{10}\right)} + 1} \tag{14}$$

The Hodgkin Huxley model was developed well before the advent of electron microscopes and computer simulations; before the work of Hodgkin and Huxley, scientists had no understanding of how the membrane of a nerve cell looked and behaved. The Hodgkin Huxley model gives structural and mechanistic explanation of a nerve cell's excitability, and it is still the central pillar in computational neuroscience.

Single neuron models can be classified into two major categories: detailed biophysical models, and simple phenomenological models. The former includes conductance-based (COBA) models following the work of Hodgkin and Huxley, known as the Hodgkin–Huxley-type models whose essence is the combination of different ion currents. Such models can successfully reproduce the complex and rich behaviors that biological neurons exhibit, as observed experimentally via intracellular electrophysiological measurements. However, simulation of a network built with such models is usually computationally expensive and analytically intractable. The latter, in contrast, are very simple models such as Boolean, binary and on/off, including McCulloch-Pitts (Graben & Wright, 2011) , and Hopfield (Hopfield, 1982) models, have been well studied and widely used in artificial neural networks.

There also exist models between the two extremes such as FitzHugh Nagumo (Izhikevich & FitzHugh, 2006) , Morris Lecar (Ditlevsen & Greenwood, 2013) , and integrate-and-fire (IF) (Burkitt, 2006). These models can be viewed as a simplification of the Hodgkin–Huxley model by reducing the original four-dimensional model to fewer dimensions, since the dynamics of membrane potential and voltage-gated conductance can be reduced as long as transmembrane conductance has fast kinetics. Fewer parameters in these models also allow simulations of large-scale networks to run quickly.

CPG and oscillations of neural networks

Oscillation is the basic kinetic model of both individual neurons and neural networks as oscillatory activity is ubiquitous in all levels of neural systems. If neurons form a network, the oscillatory activity of the neural network often arises from feedback connections between the neurons connected with excitatory or inhibitory synapses, which is a result of the synchronization of individual elements, and more complex phase relationships can arise. Synchronization and firing patterns in nervous systems play an essential role in neural signal encoding and information processing (Baars, 2010).

Central pattern generators are characterized as relatively small and autonomous neural networks, capable of generating rhythmic patterned output in the absence of sensory feedback, though sensory input is often crucial to the alternation of patterns generated and the modulation of the whole network behavior. The term “pattern” is defined to be the oscillatory behavior of a network composed of coupled neurons. There usually exists more than one pattern of oscillation in a

particular system, since a natural system is capable of switching from one pattern to another, like a horse's gait can switch from walking to trotting to bounding to galloping, which allows animal to adapt its movement to changing needs. With such characteristics, CPGs have been widely studied and an increasing number of applications of bio-inspired CPGs in control systems and robotics have emerged in the past decade (Yu, Tan, Chen, & Zhang, 2014), (Nogaret, Zhao, Moraesb, & Patonb, 2013), (Ijspeert, 2008).

The respiratory CPG of the snail

Lymnaea stagnalis (Great Pond Snail) is a kind of mollusk that lives in stagnant water and has been a classic model to study the molecular and electrical properties of neurons. It is widely used in neurobiological experiments, for its brightly-pigmented orange neurons with the feature that they can be easily identified (since they are large in size) and the ability of in vitro reconstruction of synapses and neural circuits.

The animal is a bimodal breather, which has a breathing pattern similar to that of amphibian reptiles and diving mammals. It can breathe both via skin and lung. The aerial respiration usually dominates in a hypoxic environment when the animal open and close its orifice, the pneumostome, to obtain oxygen from the air. The frequency of aerial respiration depends directly on the oxygen need (Lukowiak & Syed, 1999), and this is reflected in the firing patterns of neurons and neural networks, i.e. the respiratory CPG in this study.

The complete neural network involved in the respiration of *Lymnaea* is shown in Figure 2, including the respiratory CPG that is hypothesized to consist of only three interneurons: 1) right pedal dorsal 1 (RPeD1); 2) the input 3 interneuron (IP3I); 3) visceral dorsal 4 (VD4) and other neural connections that have influence on the aerial respiration. In this network, IP3I is said to control the aspiration through the VJ motor neurons that control the opening of the pneumostome; VD4, in contrast, controls the expiration through the VK motor neurons that control the pneumostome closure. RPeD1 receives hypoxic stimuli and modulate the frequency and firing pattern of the entire network.

By culturing the neurons *in vitro*, researchers have identified and proven that the three neurons RPeD1, IP3I and VD4, and the connections between these neurons (Figure 3) are sufficient and

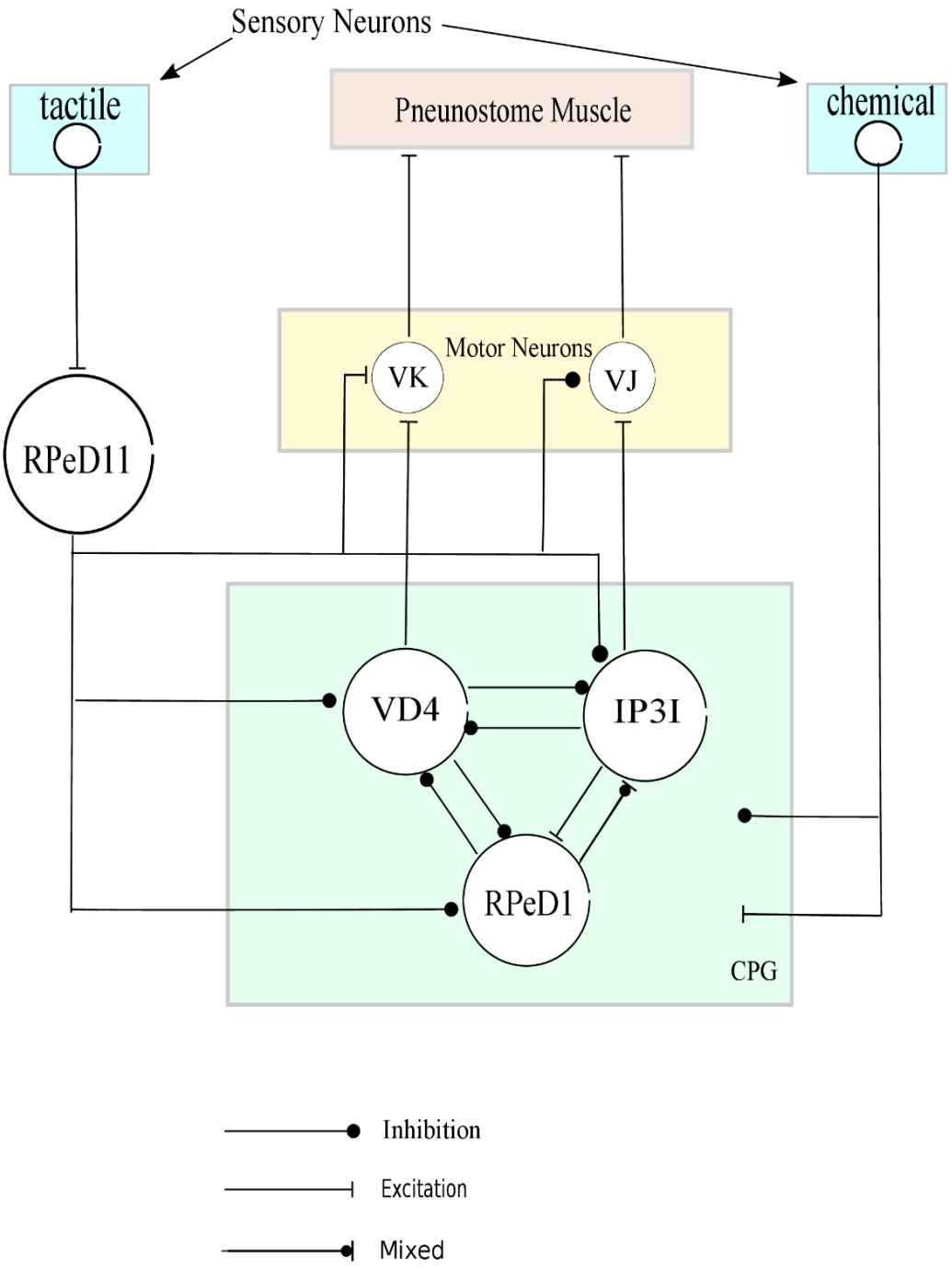

Figure 2. The complete neural circuit controlling aerial respiration, adapted from figure 1 (Taylor & Lukowiak, 2000), IP3I connects to VJ motor neurons which controls the pneumostome opening, VD4 connects to the VK motor neurons controls the pneumostome closure. The neuron RPeD11 also has inhibitory connections to all of the CPG neurons and to the VJ motor neurons, and excitatory connection to the VK neurons.

necessary to control the respiratory CPG (Syed, Bulloch, & Lukowiak, 1990). It has also been confirmed that rhythm generation is a function of emergent network properties since no single pair neurons in the CPG network was capable of generating the same rhythmic activity seen *in vivo*. Meanwhile, there also exists an argument questioning whether the VD4 neuron is involved in the respiratory rhythm generation, based on the observation of it being silent when the pneumostome closes in experiment (Vorontsov, 2002). Despite the possible involvement of other neurons in the respiratory control of *Lymanaea* and the uncertainty in the role that each neuron plays in the CPG, here we follow the observation and conclusion from Syed, Bulloch and Lukowiak (Syed, Bulloch, & Lukowiak, 1990) (Lukowiak & Syed, 1999), asserting the three neuron RPeD1, IP3I and VD4, are the only neurons necessarily involved in the respiratory control of *Lymanaea*. From their observations in vivo, RPeD1 is spontaneously active, its frequency depends on the intensity of the stimuli. During a respiratory cycle, RPeD1 first excites IP3I through post-inhibitory excitation, then IP3I fires bursts, causing the opening of the pneumostome, which excites RPeD1 but inhibitsVD4.Once recovered from the inhibitory effect of IP3I, VD4 fires bursts, causing the closure of the pneumostome, and a new cycle of respiration starts. Neither IP3I nor VD4 are endogenous bursters as they are mostly quiescent except during active respiration.

The *in vitro* experiments revealed more about the behavior of individual neurons as well as the interactions between the two bursting neurons (Syed, Bulloch, & Lukowiak, 1990). IP3I and VD4 can also fire alternating bursts when phasic but not when constant dopamine is injected (Figure 4). The bursting patterns of these two neurons observed from the in vitro recording are almost indistinguishable, which may imply that the inner properties of IP3I and VD4 are similar or identical. Moreover, given that the RPeD1 neuron is a giant dopamine neuron, it is suggested that the neurotransmitter dopamine, which is commonly associated with reward systems and addiction in the human brain, might affect the excitability of the IP3I and VD4 neurons, and play an essential role in rhythm generation.

Bursting and the richness of behavior of neurons

The Hodgkin-Huxley mechanism illustrated that ion channels determine the behavior of neurons. Because of the diversity and variety of ion channels, individual neurons show exceeding richness

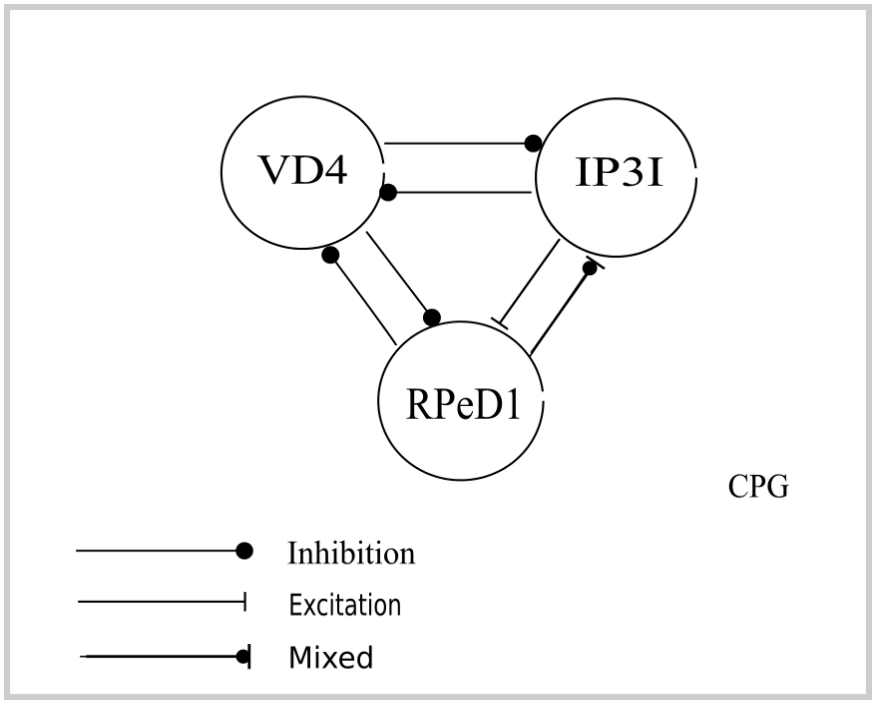

Figure 3. The respiratory CPG of Lymnaea consisting of 3 neurons. RPeD1 is a giant dopamine neuron with a mixed inhibitory-excitatory connection to IP3I, while IP3I has excitatory connection to RPeD1. VD4 and RPeD1 have reciprocal inhibitory connections to each other, as do VD4 and IP3I.

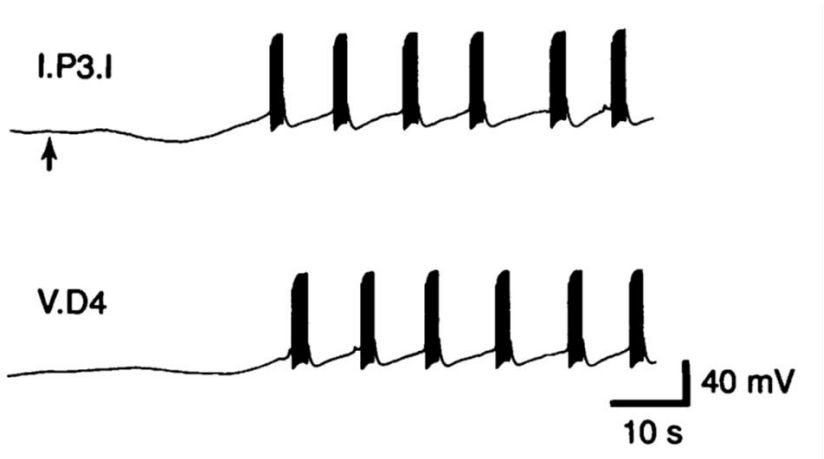

Figure 4. Alternating bursts of coupled IP3I and VD4 neurons cultured in vitro without RPeD1 when phasic dopamine is applied (beginning at the arrow). The continuous presence of dopamine cannot elicit the same bursting behavior; the phenomenon is seen as evidence of the necessity of the presence of the dopamine neuron RPeD1. Adopted from Figure 4 (Syed, Bulloch, & Lukowiak, 1990). Reprinted with permission from AAAS.

and complexity of spiking behavior. Twenty of the most prominent features (Figure 5) of biological spiking neurons are summarized and categorized by studying the computational features of neuron models with respect to their biological plausibility and computational efficiency (Izhikevich, 2004). It is notable that the 20 classifications listed in Figure 5 are generated by the same model with different choices of parameters, which shows the potential of using adequate mathematical models to reduce complexity while retaining desired output patterns. This sparks an interest in modelling biological neural networks with existing general neuron models.

Without discussing all neuronal behaviors and the biophysical mechanisms behind in an adequate detail, instead, we focus on the bursting behavior as observed in the aforementioned CPG network. Bursting is characterized as periods of rapid spiking followed by quiescent periods. Bursts are generally viewed as a way of increasing the reliability of communication, or as a unit of neuronal information in selective communication between neurons, based on the observation that the same burst can resonate for particular synapses or cells but not for others, depending on their natural resonance frequencies (Izhikevich, et al., 2003). Several hypotheses have been formulated regarding the importance of bursting activity in neural computation; for example, 1) selective communication if the cells are sensitive to the frequency content of the input; 2) higher signal-to-noise ratio that overcomes noise in single spikes; 3), encoding different features from sensory input (Izhikevich, 2006). There are 4 computational properties commonly used to depict and quantify a burst: Duty Cycle, Amplitude, Number of Spikes per burst and Inter-Spike Interval (ISI) (Figure 6).

Dynamical systems theory, especially bifurcation theory is commonly applied when classifying particular behaviors of neuron models. For instance, a more detailed classification of bursting oscillations based on phenomenology focuses on

1) Spike frequency, how the spike frequency changes in a burst
2) Shape and morphology of a burst, such as whether undershoot or plateau exist in the spikes

which can be linked to the analysis of the topology of phase plane and bifurcation diagrams using dynamic system theories (Bertram R, Butte, Kiemel, & Sherman , 1995).

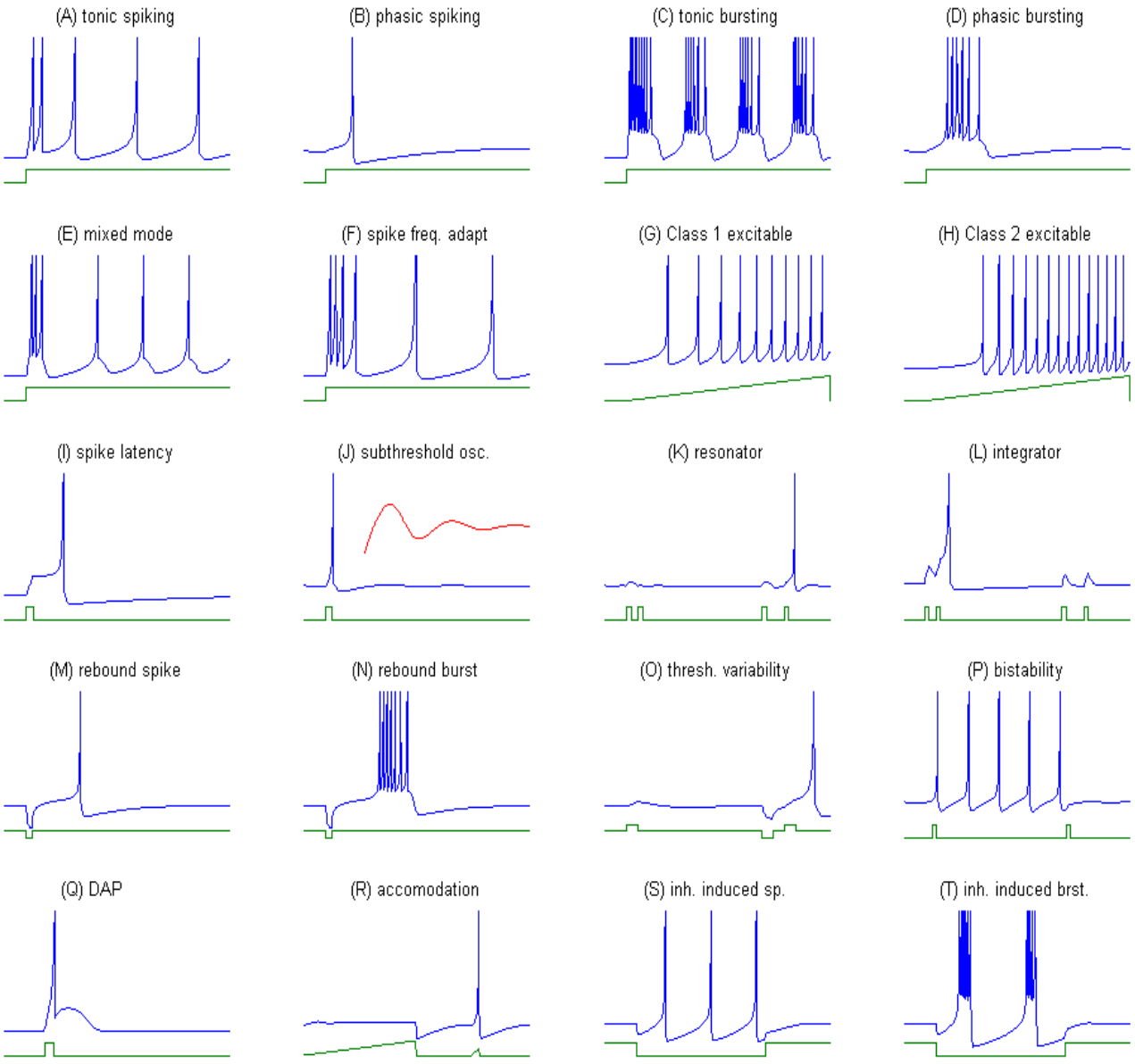

Figure 5, Behavior of biological spiking neurons in response to DC current stimulus, adapted from Figure 1 (Izhikevich, 2004). The MATLAB file generating the figure is from ModelDB, Artificial neuron model (Inhikevich 2003), Accession: 399948 (http://senselab.med.yale.edu/modeldb/showmodel.asp?model=39948)

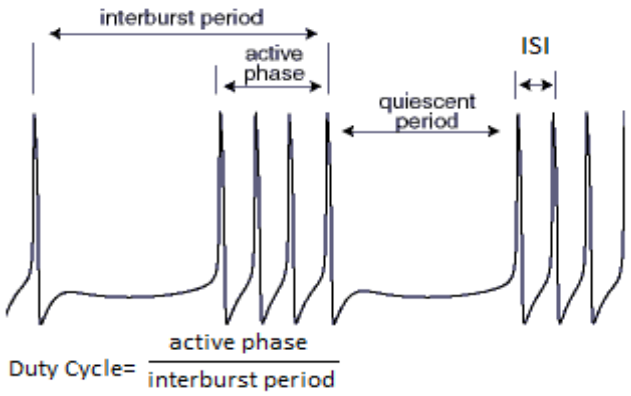

Figure 6. Computational properties of the bursting activity in neurons. The term duty cycle, used to describe waveforms in electronics, refers to the percentage of the ratio of pulse duration to the total period of the waveform.

Methods

The artificial CPG is hypothesized to consist of a pacemaker neuron and a Half-Center Oscillator (HCO) as in the biological CPG, as well as a total of six synaptic connections between these neurons. In the context of a living brain, the pacemaker neuron RPeD1 is responsible for receiving sensory feedback from the outside environment and regulating the rhythmic patterns of the HCO, in fact, the entire neural network. However, the intracellular mechanism of each neuron, even the entire CPG, remains unclear, though we have basic knowledge of the connections between the neurons and the behavior of each neuron coupled and uncoupled. Ideally, if all of the information on the inner ion channels of the three neurons and their synaptic connections are derived from experimental data, we can build a detailed HH-type computational model that closely mimics the individual neurons and the real neural networks. For example, the COBA type RPeD1 neuron model (Bungay & Campbell, 2009), and the snail feeding CPG network model (Vavoulis, et al., 2007). These models are biologically meaningful as they faithfully depict the output behavior and the inner mechanisms based on sufficient knowledge of the ion channels involved. On the other hand, such models require much highly accurate experimental data which is difficult to obtain; meanwhile, the resulted system could be complicated and expensive to implement computationally due to its high dimension. Therefore, we decide to build the artificial CPG from existing neuron models and make the assumption that IP3I and VD4 are identical since their behavior is quite similar in the original respiratory CPG. We choose the 2D Morris-Lecar model as the basic single neuron model for the three neurons in the network to maintain a consistent time scale for the

neurons when coupled and uncoupled. This model incorporates both potassium and calcium currents, and an additional T-type current has been added in the HCO model for bursting neurons. Parameter values are adjusted to achieve similar behavior as observed in the biological CPG. The neurons are coupled via synapse models and adjusted with the introduction of time delay to the synaptic gating variable in the synapse model.

The models are described below in the following order:

1) Single neuron model of the RPeD1 neuron
2) Single neuron model of the HCO
3) Model of synapse
4) Model of the CPG network as ODE system
5) Synapse delay

Model of pacemaker neuron RPeD1

The single neuron model is built to represent RPeD1's tonic spiking behavior when coupled and uncoupled.

$$C\frac{dV}{dt} = -g_{Ca}m_{\infty}(V - V_{Ca}) - g_K w(V - V_K) - g_L(V - V_L) + I_{app} \tag{15}$$

$$\frac{dw}{dt} = \phi\frac{w_{\infty} - w}{\tau_w} \tag{16}$$

where

$$m_{\infty} = \frac{1 + tanh\frac{V - V_1}{V_2}}{2} \tag{17}$$

$$w_{\infty} = \frac{1 + tanh\frac{V - V_3}{V_4}}{2} \tag{18}$$

$$\tau_w = \text{sech}\left(\frac{V - V_3}{2V_4}\right) \tag{19}$$

V denotes the membrane potential, C is the capacitance of the cell membrane, w is the recovery variable and denotes the probability that the potassium channel is conducting, g_{Ca}, g_K and g_L are the peak conductance of calcium, potassium, and leak channel respectively, and V_{Ca}, V_k and V_L are

the equilibrium potentials of the respective ion channels. The open-state probability functions m_∞ and w_∞ are derived from experimental observation of open and closed states of a channel where V_1, V_2, V_3 and V_4 are constants also derived from experimental data. ϕ is the temperature factor which speeds up the activation rate for increasing temperature (Borisyuk, 2014).

Model of HCO bursting neurons

The HCO model is adapted from a pair of bursting neurons with reciprocal inhibition (Matveev, Bose, & Nadim, 2007). The two cells are assumed to be identical and the Morris-Lecar model is modified to add a low-threshold calcium current, i.e. the T-current. The T-current is responsible for the bursting behavior and can be modeled as

$$I_T = g_T a h (V - V_{Ca}) \tag{20}$$

where g_T is the peak conductance of the T-current. Since the activation is faster than inactivation kinetics for the T-current, the activation variable a can be descried as a Heaviside function,

$$a = H(V - V_h) = \begin{cases} 0 & V \leq V_h \\ 1 & V > V_h \end{cases} \tag{21}$$

and the inactivation variable h dependent of time constants τ_{low} and τ_{hi} is described by

$$\frac{dh}{dt} = \begin{cases} \dfrac{1-h}{\tau_{low}} & V \leq V_h \\ -\dfrac{h}{\tau_{hi}} & V > V_h \end{cases} \tag{22}$$

Both the activation and inactivation thresholds are set equal to V_h. The discontinuity in the Heaviside functions is smoothed in numerical simulation using the sigmoidal function

$$\sigma(V - V_h) = \frac{1}{2(1 + \tanh(4(V - V_h)))} \tag{23}$$

Model of synaptic connection

Chemical synapses function in a way that when the presynaptic neuron is activated (usually seen as firing spikes) and releasing vesicles, the effect on the postsynaptic neuron is an exponential decay corresponding with the decline in concentration of neurotransmitters released. For simplicity, this process is usually modelled as transmitter-activated ion channels with time-

dependent conductivity when a presynaptic spike arrives, instead of the neurotransmitter concentration. The synaptic current I_{syn} from neuron i to j is modeled as

$$I_{syn} = g_{syn} s_{ij} \left(V_j - V_{syn}\right) \tag{24}$$

$$\frac{ds_{ij}}{dt} = \begin{cases} -\dfrac{s_{ij}}{\tau_{syn}}, & V_i \le V_\theta \\ \dfrac{1 - s_{ij}}{\tau_g}, & V_i > V_\theta \end{cases} \tag{25}$$

where g_{syn} is the peak conductance of the synaptic current, V_j denotes the membrane potential of neuron j, $V_{syn}$is the reversal potential which can be either excitatory or inhibitory, s_{ij} is the synaptic gating variable (which is also smoothed using sigmoidal function $\sigma(V - V_\theta)$ during numerical simulation), V_θ is the spike threshold of neuron i and set as constant, and τ_{syn} and τ_g are synaptic decay time constants associated with the intrinsic properties of neuron i.

The synaptic connections defined in the CPG model all follow the same type of inhibition or excitation as in Figure 3, both excitatory and inhibitory synapse are modeled as in Equation (24). For the excitatory synapse, the reversal potential V_{syn} is set to the value of -20; while for the inhibitory synapse the value is -80. For simplicity, the post-inhibitory excitation between RPeD1 and IP3I is treated as an excitatory synapse and its synaptic reversal potential is set to be the same value as the excitatory synapse. With this configuration, the network contains only two types of neurons and two types of synapses.

Model of network

The network consists of the models of 3 neurons and 6 synapses with certain parameters adjusted in order to obtain desired behaviors. Neuron 0 denotes the pacemaker neuron RPeD1, neuron 1 and 2 denote IP31 and VD4 which are identical.

$$C\frac{dV_0}{dt} = I_{app} - I_L - I_{Ca} - I_K - I_{syn_{10}} - I_{syn_{20}} \tag{26}$$

$$C\frac{dV_1}{dt} = I_{app} - I_L - I_{Ca} - I_K - I_T - I_{syn_{01}} - I_{syn_{21}} \tag{27}$$

$$C\frac{dV_2}{dt} = I_{app} - I_L - I_{Ca} - I_K - I_T - I_{syn_{02}} - I_{syn_{12}} \tag{28}$$

Introduction of delay

Delay-differential equations (DDEs) are characterized as the derivatives of functions at the present being dependent on the values at previous times. DDEs have been applied to many areas of engineering and science, especially control systems to describe the inherent time delay phenomenon in closed-loop feedback systems. Previous studies have shown the usefulness of DDEs in studying neural networks (Lu, Wang, & Shi, 2009), (Coombes & Laing, 2009). Thus, for better control of timing, two delays are introduced in the synaptic gating variable s_{12} and s_{21}. The synaptic gating variable s_{ij} is dependent on the membrane potential V_i, which can be written as

$$\frac{ds_{ij}}{dt} = f\big(V_i(t)\big) \tag{29}$$

When a delay τ is introduced, the above equation can be written as

$$\frac{ds_{ij}}{dt} = f\big(V_i(t-\tau)\big) \tag{30}$$

With delay introduced to the system, the original ODE system becomes a DDE system and is capable of providing better control of timing for the artificial CPG.

Results

Neuron models derived from Hodgkin-Huxley type model are described as a set of differential equations that relate function with its derivatives and need to be solved numerically. Two types of differential equations, ordinary differential equations (ODEs) and delay-differential equations (DDEs) are presented in our modelling. All simulations are run in the Matlab software environment.

Model analysis

The pacemaker RPeD1 neuron is modeled by a Morris Lecar model with parameters corresponding to Type 1 excitability. The classification of neuron excitability was first studied by Hodgkin (Hodgkin 1948). Type 1 excitability corresponds with a continuous frequency-current (*f-I*) curve, neurons in this class are capable of spiking repetitively across a broad range of rates. On the other

hand, Type 2 excitability corresponds with a discontinuous *f-I* curve, neurons in this class fire

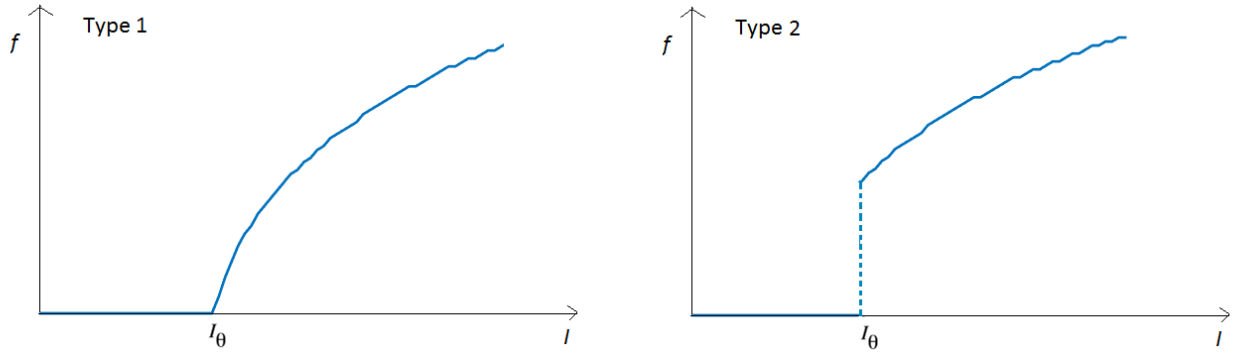

Figure 7. Type 1 and Type 2 excitability. The frequency-current (f-I) curve is continuous for Type 1 neurons, and discontinuous for Type 2 neurons.

across a narrower range and are not capable of maintaining slow repetitive spiking (Figure 7). By analyzing the computational model of RPeD1 neuron created by Bungay and Campbell (Bungay & Campbell, 2009), which is a conductance-based Hodgkin-Huxley model and considered to be biologically meaningful and measurable, we suggest that RPeD1 falls into the category of Type 1 excitability (Figure 8). In this model, the neuron fires tonic spiking without an applied current, and the frequency increases as the intensity of the external current increases. However, if the injected current is negative, it prevents the neuron from tonic spiking (i.e. the threshold current is negative), which is different from the Morris-Lecar model based RPeD1 neuron since its threshold current I_θ is non-negative (Figure 9).

Comparing the tonic spiking behavior and *f-I* curve of the two models (Figure 10, Figure 11), we consider the Type 1 Morris-Lecar model based RPeD1 a reasonable choice for building the artificial CPG. Besides the consideration on morphology and waveforms of spiking behavior, the frequency and time scale are also key factors that cannot be neglected in modelling. It is notable that the two models vary significantly as seen in Figures 10 and 11. The RPeD1 neuron spikes with a very low frequency in the real-world environment while the Morris-Lecar model has a much higher frequency. Since when multiplied by a scaling factor, linear transformation of time scale and the amplitude of voltage are both achievable for output, this is not considered to be a problem for modelling at this stage serving the goal of visualization. If the output of the artificial CPG is applied to controlling certain systems requiring accurate pacing, the linear transformation of time should be considered.

The primary goal of this study is to approach the output patterns observed in the biological CPG network as much as possible on a computer. The original biological CPG has been studied by neuroscientists both *in vivo* and *in vitro* (Syed, Bulloch, & Lukowiak, 1990), and the recording of the network with the three neurons' firing pattern (shown in Figure 12) illustrates the behavior that

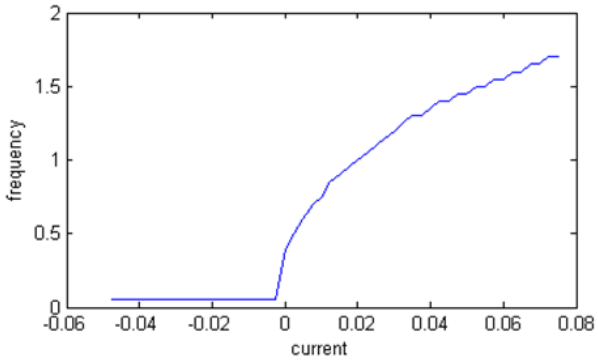

Figure 8. f-I curve of the computational model of RPeD1 neuron created by Bungay and Campbell (Bungay & Campbell, 2009)

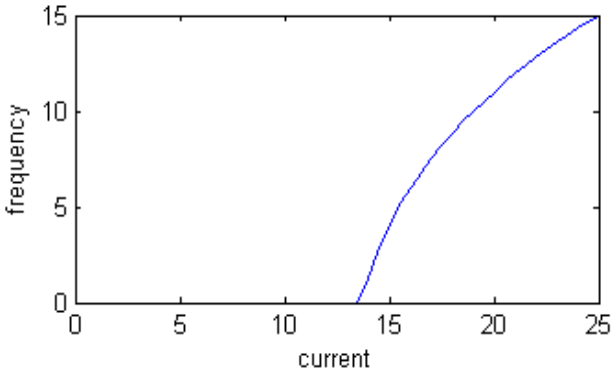

Figure 9. f-I curve of the Morris-Lecar Model based RPeD1 neuron in the artificial CPG

the artificial CPG model attempts to replicate. From the recording of voltage trace (Figure 12), it is clear that the duty cycle of the two bursting neurons IP3I and VD4 is the same, around 0.12 – 0.15. In the real-world context, the duty cycle of each bursting neuron is expected to decrease until the neurons stop firing burst once anaerobic stimuli are removed, which corresponds to the scenario that the respiration cycles start with a more intense breathing pattern when the snail encounters a shortage of oxygen at the beginning and the frequency then slows down as the snail gradually relieves that shortage, and eventually stops breathing with its lung. These two neurons are hypothesized to form an HCO due to the reciprocal inhibition between them. An HCO model studied by Matveev et.al focusing on discovering the relationship between the inter-spike interval (ISI) and bursting length (Matveev, Bose, & Nadim, 2007) was chosen as the prototype of the HCO model for IP3I and VD4 in the CPG. Some of the parameters are modified to achieve the desired behaviors. For instance, if the leak channel conductance increases to a particular value, we are able to obtain a quiescent period (Figure 13) after active phase compared to the original CPG without a quiescent period with a lower leak channel conductance (Figure 14).

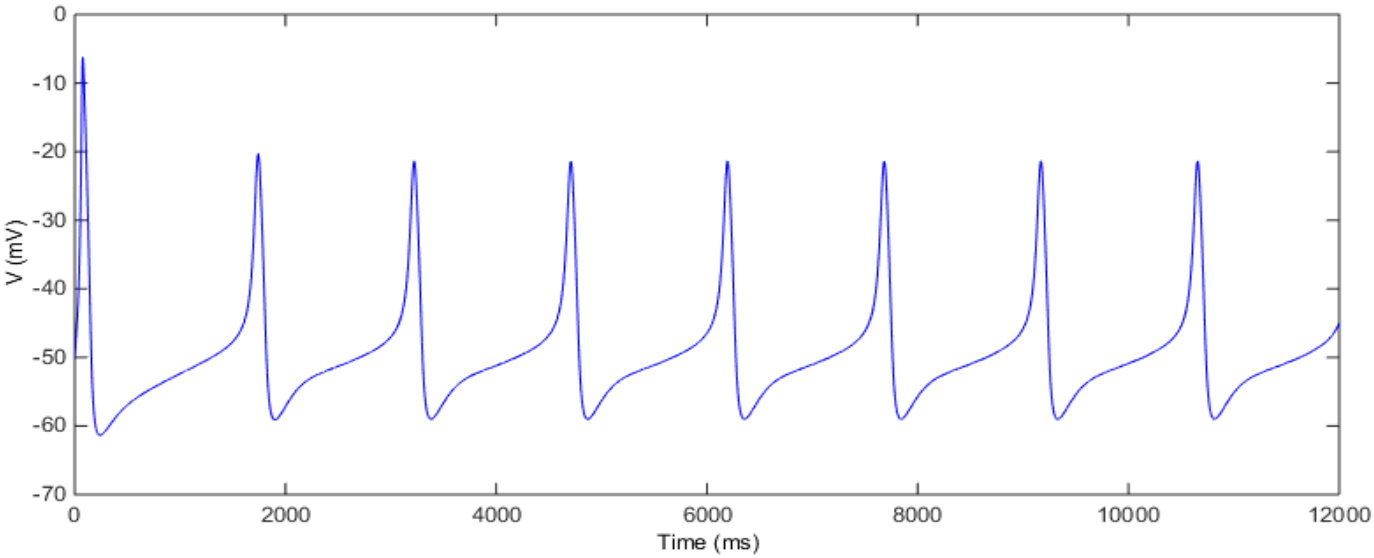

Figure 10. Tonic spiking of the conductance-based RPeD1 neuron when applied current equals 0, as the RPeD1 neuron in the CPG fires tonic spiking spontaneously.

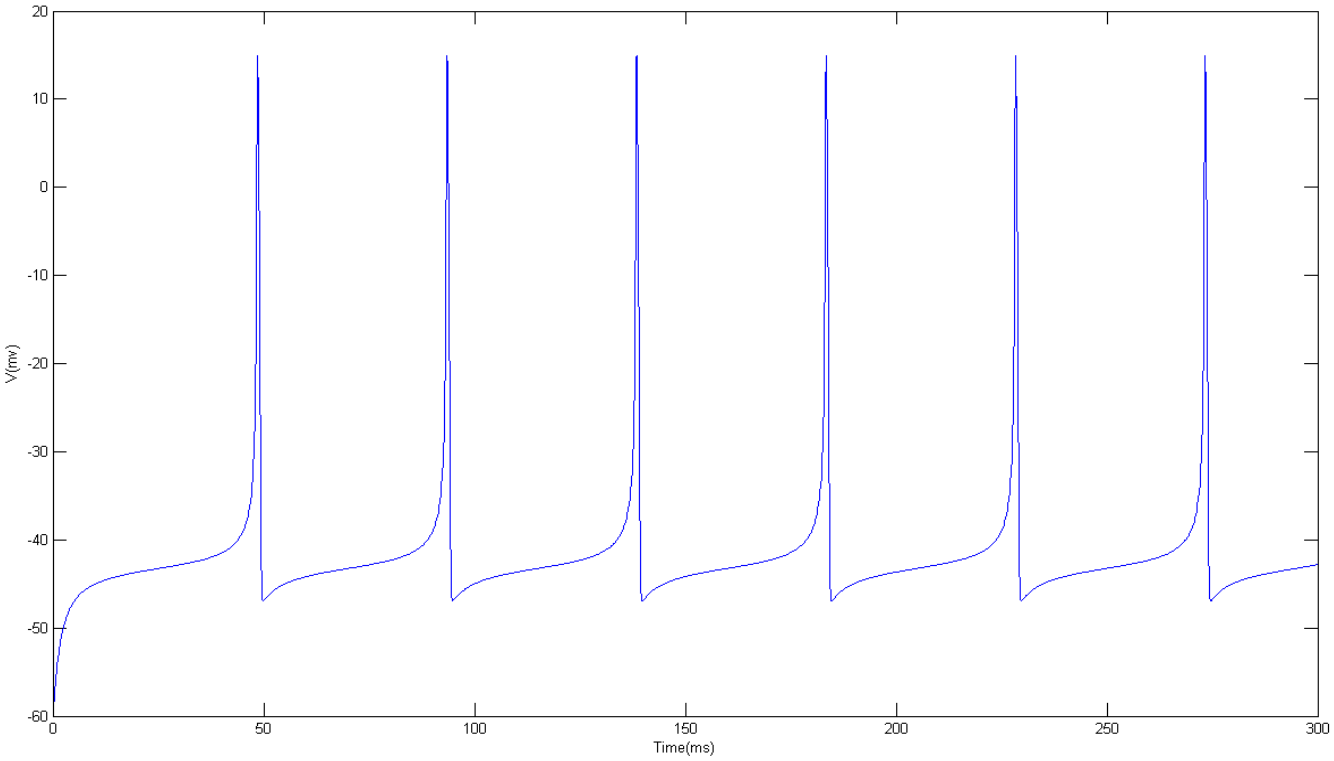

Figure 11. Tonic spiking of Morris-Lecar with parameters corresponding with Type 1 excitability. Applied current =14.

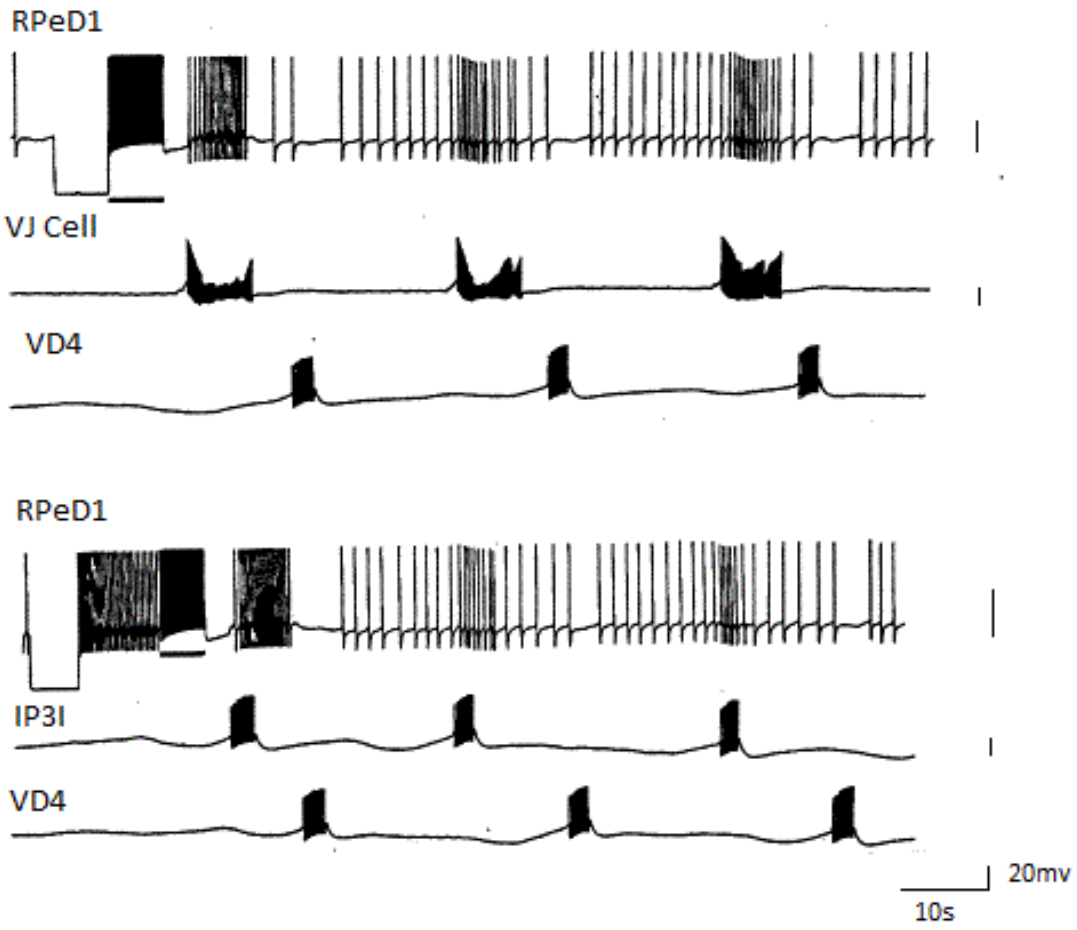

Figure 12. In vivo and in vitro recording of the three neurons in the CPG, Adopted from figure 3 in the research paper "In vitro reconstruction of the respiratory central pattern generator of the mollusk Lymnaea" by Syed, Bulloch and Lukowiak (Syed, Bulloch, & Lukowiak, 1990). Reprinted with permission from AAAS. The top figure depicts the simultaneously recording of the stimulated network in vivo, and the bottom figure depicts the recording in vitro. IP3I is difficult to locate in the context of isolated brain preparation, instead, its follower, the Visceral J cell (V.J cell) was being recorded in the top figure.

The duty cycle of the HCO is around 0.4 in Figure 13 when the leak channel conductance g_L is set to 3.0; however, it is impossible to elongate the quiescent period by merely increasing the leak channel conductance g_L while still preserving the alternating bursting pattern in the ODE system as large g_L values will break the alternating bursting pattern of the HCO.

Changing certain parameters leads to a different behavior for neurons, such as adjusting the leak channel conductance g_L results in a quiescent period after active phase in the HCO bursting neuron model (Figure 13, 14). The inner mechanism of how these changes affect the behavior of neurons

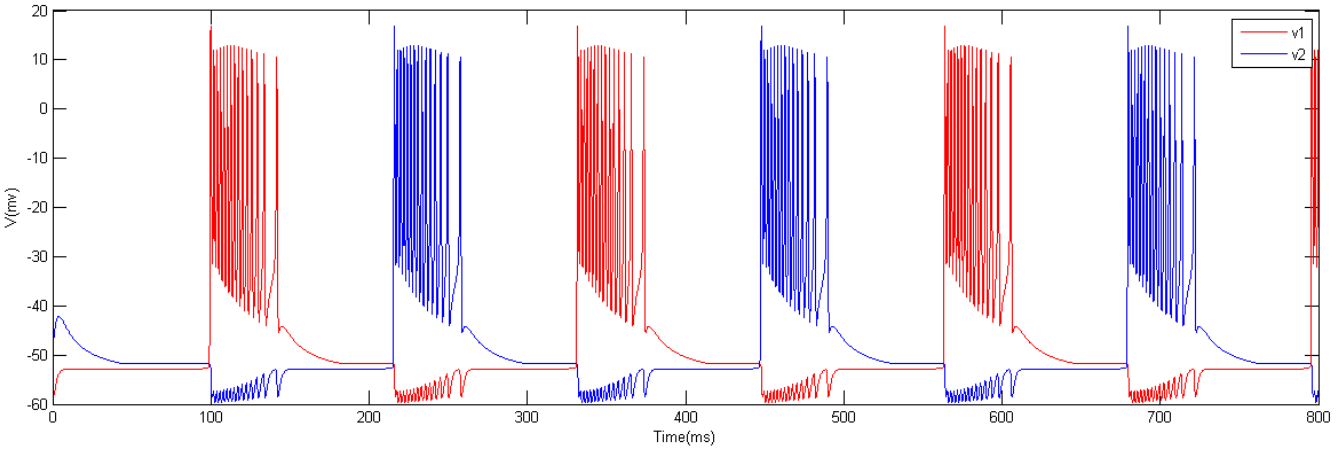

Figure 13. Increase the leak channel conductance gL to 3.0, to obtain a quiescent period after active phase in the HCO model as an ODE system without delay. The two neurons and the two inhibitory synaptic connections are identical. v1 and v2 denote the voltage of the two neurons, the initial conditions of the two neurons are not identical.

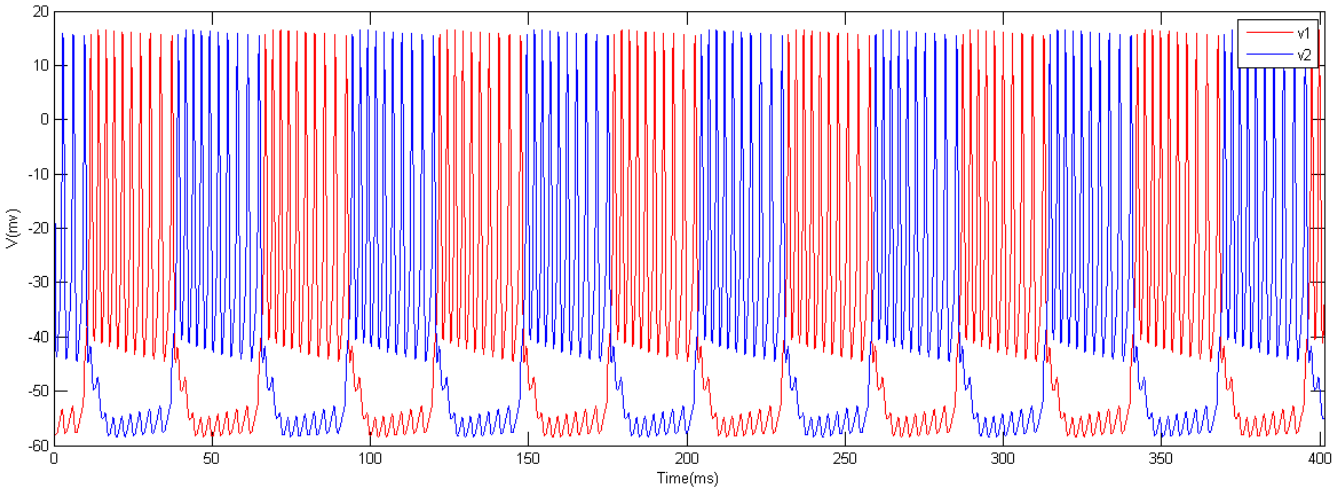

Figure 14. Prototype HCO model firing alternating burst without quiescent period. The leak channel conductance gL in the prototype HCO model equals to 2.0. Different choices of initial conditions for the two neurons can give different numbers of spikes per burst.

is unclear to us and needs further exploration; for example, using bifurcation analysis, which can determine the types of dynamic behaviors that exist in the system, as well as the range of the parameter values for maintaining a stable firing pattern. Intuitively, the observed quiescent period brought by a larger leak channel conductance (Figure 13) may indicate that the leak current plays a special role in the Morris-Lecar Model (González-Miranda, 2014).

Artificial CPG model of ODE system

By the construction of a 14D ODE system combining the pacemaker neuron model and the HCO model, the artificial CPG is able to produce similar output as in the biological CPG; however, it cannot fully replicate the rhythmic pattern with respect to control of timing, such as the duty cycle, due to a limited synaptic regulation. Figures 15 and 16 show the output of the constructed artificial CPG as an ODE system, V_0 represents the membrane potential of RPeD1 neuron, V_1 and V_2

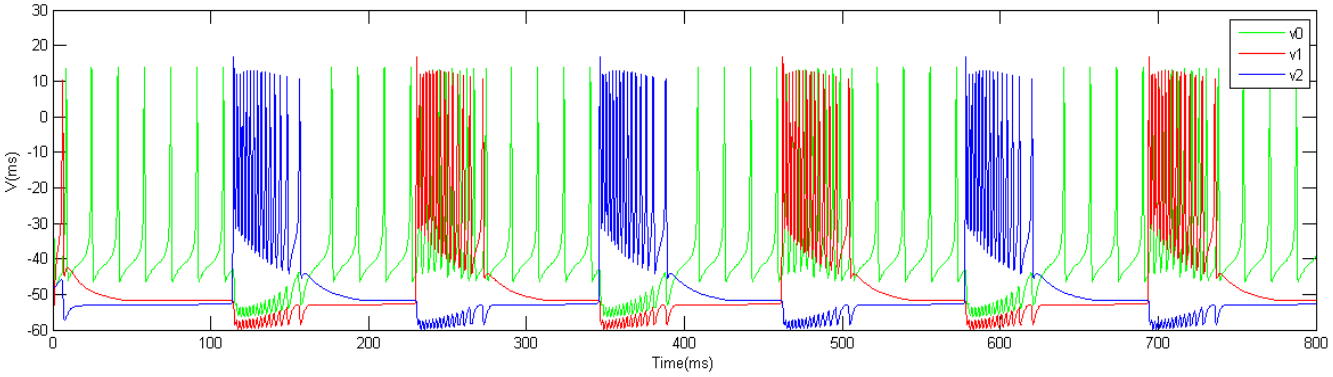

Figure 15, Output of the ODE system (overlapped view). The ODE system of the artificial CPG consisting of the HCO model of two identical bursting neurons and a tonic spiking Morris-Lecar model. V_0, V_1 and V_2 denote the membrane potential of RPeD1, IP3I, VD41

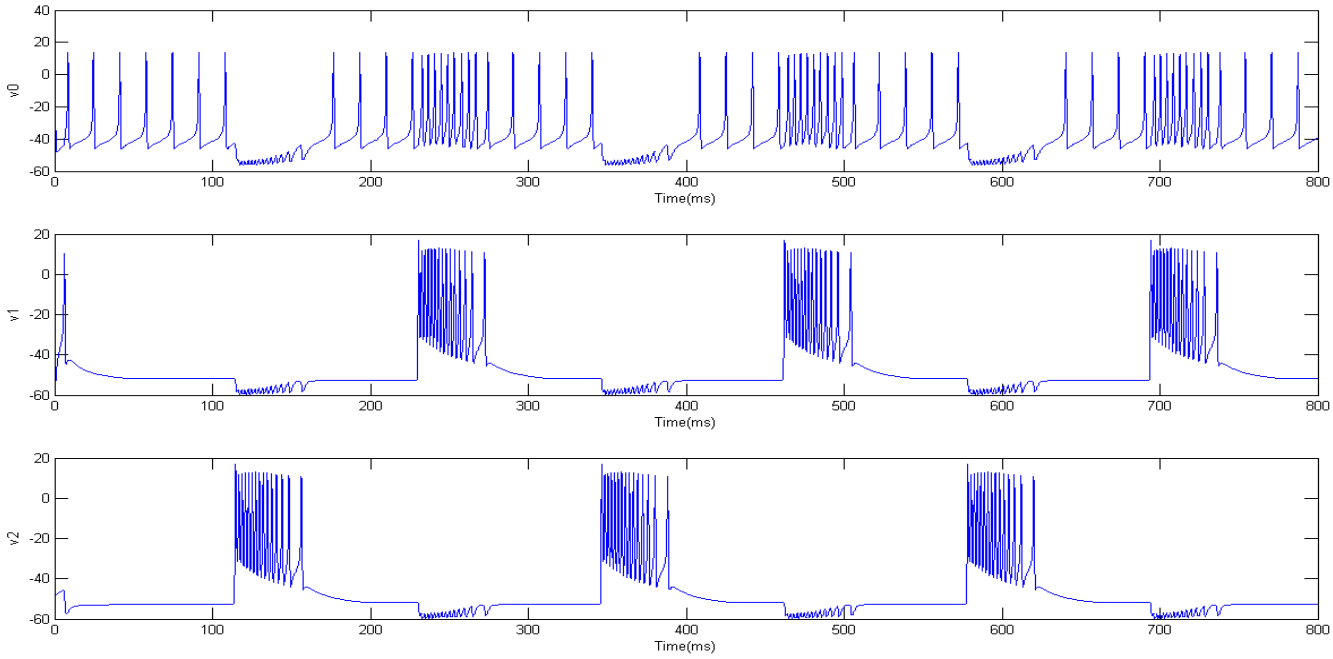

Figure 16, Output of constructed ODE system (separate view). V0, V1 and V2 denote the membrane potential of RPeD1, IP3I, VD41 respectively. The system demonstrates a similar firing pattern as seen in Figure 12.

represent IP3I and VD4 respectively.

In Figures 15 and 16, the synaptic threshold V_{θ_0} (Equation 25) of the RPeD1 neuron that affects the synaptic variables s_{01} and s_{02} is set to be 15 or higher, significantly larger than the synaptic threshold V_θ of the HCO neurons IP3I and VD4 which is equal to -3 (the default synaptic threshold value as used in Figure 13 and 14). This adjustment of the synaptic threshold in RPeD1 is made to

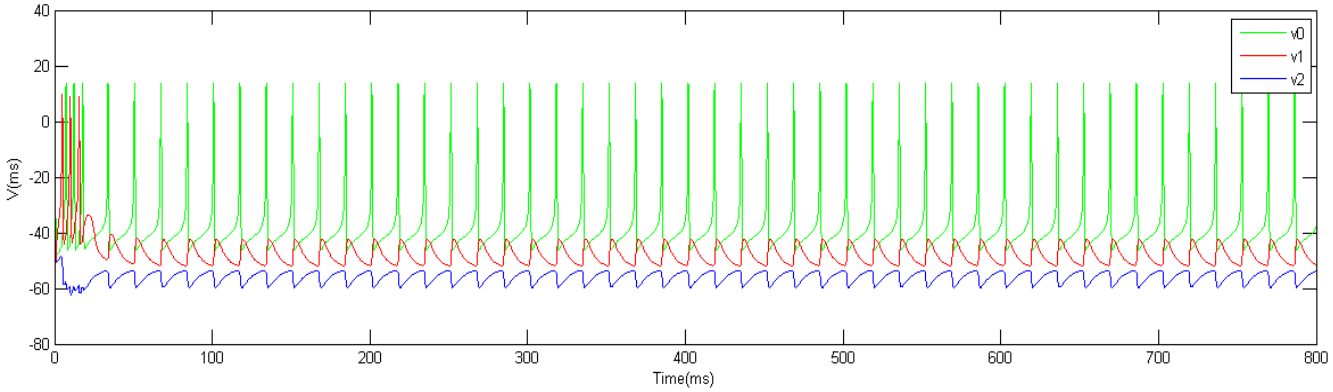

Figure 17, A lower synaptic threshold V_{θ_0} = 0, results in a different firing pattern of the network and breaks the alternating bursting in HCO. All other parameters remain the same compared to those in Figure 15 and 16. V0, V1 and V2 denote the voltage trace of RPeD1, IP3I and VD4 respectively.

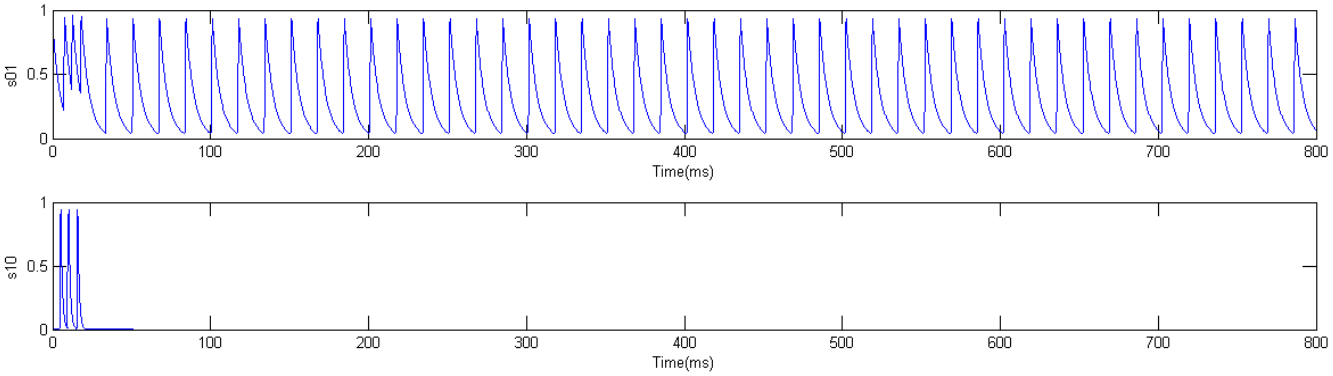

Figure 18,Time trace of synaptic gating variables s01 and s10 with the same parameter setting as in Figure 17, when the synaptic threshold V_{θ_0} of RPeD1 is set as 0, the synapse s01 from RPeD1 to IP3I is functioning while s10 from IP3I to RPeD1 is not.

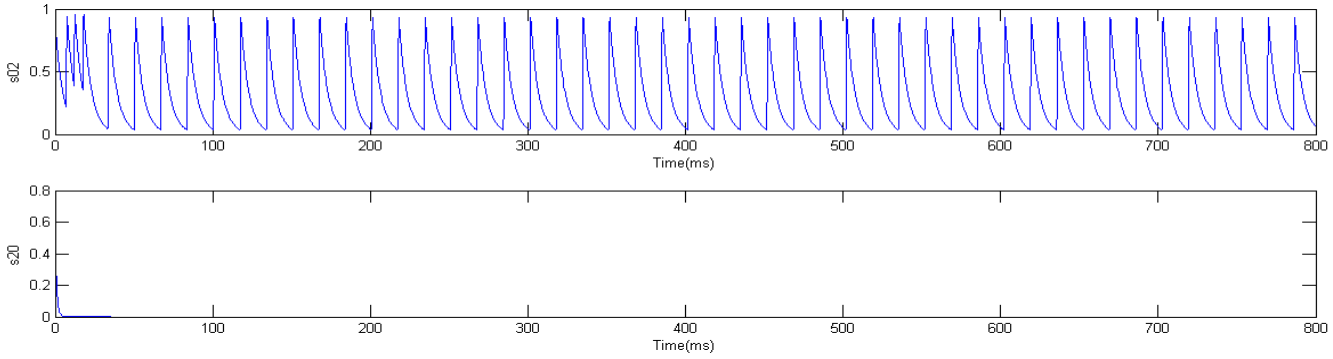

Figure 19, Same parameter setting with Figure 17 and 18, time trace of synaptic gating variables s02 and s20, when the synaptic threshold V_{θ_0} of RPeD1 is set as 0, it is similar to Figure 18 that s02 from RPeD1 to VD4 is functioning while s20 from VD4 to RPeD1 is not functioning.

achieve the firing patterns of the desired network (Figure 12), because any lower synaptic threshold results in a quite different regime (Figures 17, 18 and 19), which is caused by the lack of synaptic input from the HCO to RPeD1.

Such configuration can be seen as a compromise for the synapse model defined in Equation 24, 25,

$$I_{syn} = g_{syn} s_{ij} (V_j - V_{syn}) \tag{24}$$

$$\frac{ds_{ij}}{dt} = \begin{cases} -\frac{s_{ij}}{\tau_{syn}}, & V_i \le V_\theta \\ \frac{1 - s_{ij}}{\tau_g}, & V_i > V_\theta \end{cases} \tag{25}$$

where a higher threshold set beyond the peak voltage of the neurons means that V_i is always smaller than V_θ, results in a single decay formula and limited synaptic effect from neuron i. Consequently, while rising the synaptic threshold of RPeD1, the HCO will dominate and maintain a similar firing and bursting pattern, since the pacemaker neuron cannot regulate the HCO with weak synaptic effect. This observation may imply that our model is overly simplified compared to the original CPG and the synapse model should also be adjusted. This fact indicates the necessity of bringing other factors to the HCO in order to control the timing of the entire network; therefore, delay is incorporated into the system instead of rebuilding the model of the whole network.

Artificial CPG model of DDE system

To overcome the aforementioned problem of lack of timing control in the ODE system of the artificial CPG, delay is introduced in the system. With the introduction of two delays in the synaptic gating variables s_{12} and s_{21} in the HCO, the entire period is elongated as the quiescent

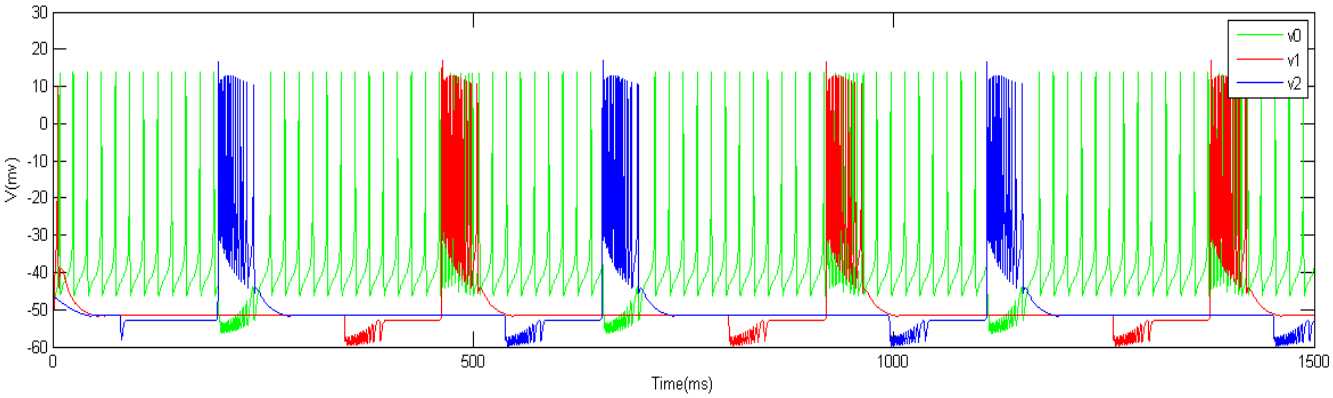

Figure 20, Output of constructed DDE system with two delays in the synaptic gating variable s12 and s21, the delays were set to75 and 150 ms respectively, v0= RPeD1, v1=IP3I, V2 = VD4, (overlapped view).

period increases, the output of the artificial CPG also approaches the behavior of the original CPG better as shown in Figures 20 and 21. The values of the delays were chosen to be 75 and 150 ms respectively based on period to conform to the asymmetric firing pattern in Figure 12.

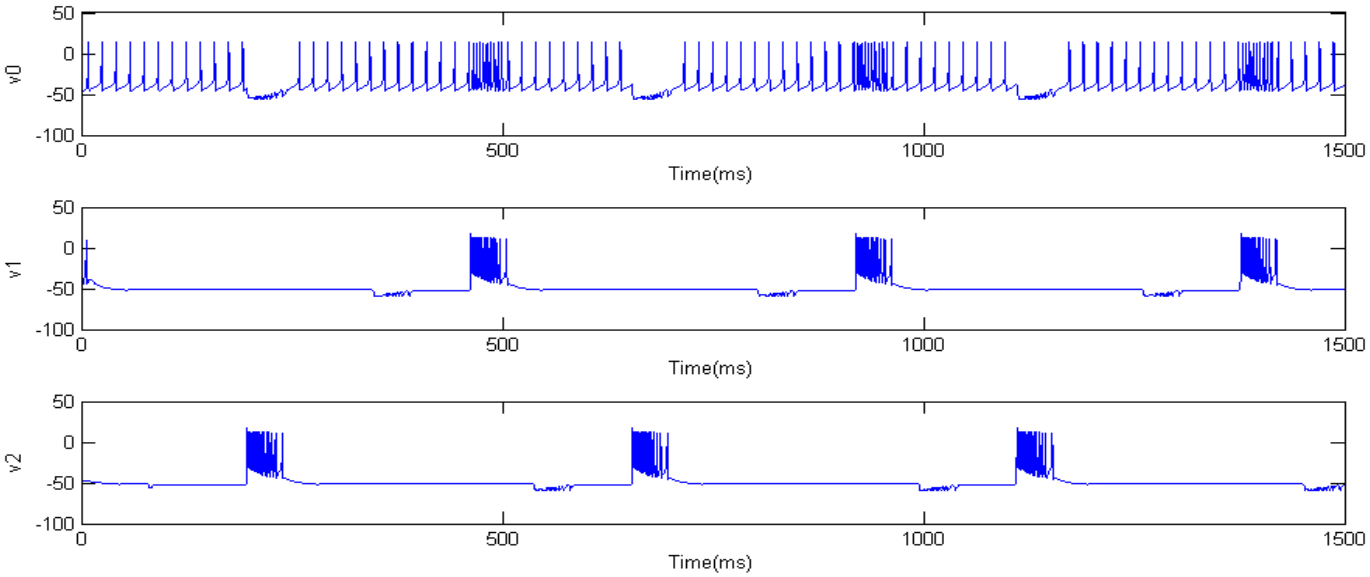

Figure 21, Output of constructed DDE system with 2 delays in the synaptic gating variable s12 and s21, the delays were set to 75 and 150 ms respectively, v0= RPeD1, v1=IP3I, V2 = VD4. (separate view).

Since we added two delays, the ratio of the two delays is capable of controlling the position of the active burst period that each neuron presents in the output pattern. For instance, if we set the two

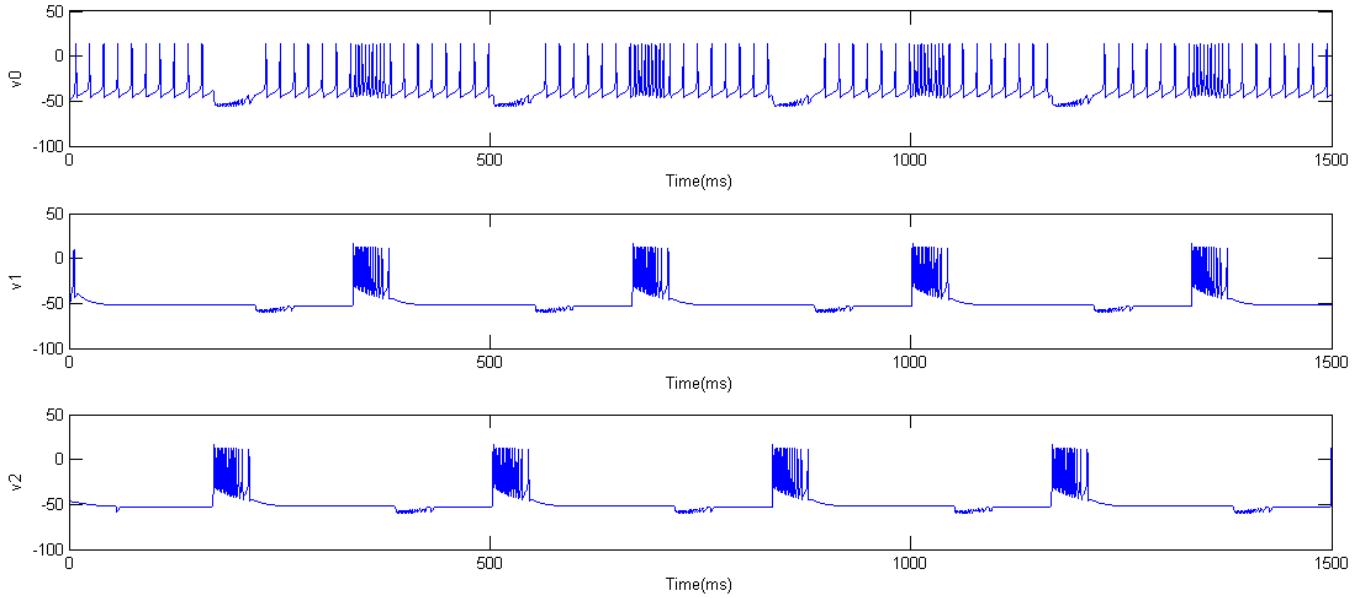

Figure 22, Output of constructed DDE system with 2 delays of the same value 50 ms in the synaptic gating variable s12 and s21, v0= RPeD1, v1=IP3I, V2 = VD4, (separate view).

delays to be the same value of 50 ms (Figure 22), the VD4 neuron (marked as V2) bursts at the middle of the interburst period of the IP3I neuron (marked as V1), rather than at the section close to the left end of the interburst period, around 1/3 part, as in Figure 21. On the other hand, the length of the delays affects the period of the entire neural network but not the active phase of the bursting. After observing that the HCO dominates the period and output pattern of the neural network ODE system, we assume that adding the delays to the synaptic gating variables of the HCO bursting neurons will be the most effective for controlling the timing and period, and the simulations proved the feasibility and effectiveness of adding the time delays in the synaptic gating variables of the HCO.

Discussion

With respect to the CPG, there is not yet a well-established design method, some possible approaches explored by previous researchers can be categorized into three classes: hand-coding, designs based on dynamical systems theory, and those using learning/optimization algorithms (Ijspeert, 2008). The modelling process in this study is based on knowledge of existing neuron models and numerical simulations. To summarize, firstly, based on assumptions and analysis, we defined the topology and structure of the network by dividing the network to two parts: a pacemaker and a HCO; secondly, we chose models whose behaviors resemble the original behaviors of each part based on the waveforms; thirdly, the two parts were coupled together as a 14D ODE system that preserves the oscillatory pattern of the network; fourthly, delay was introduced and the ODE system became a DDE system which allows flexible control of timing.

In terms of whether an artificial CPG can provide better understanding of biological CPG, it is unlikely to be certain for our model due to a lack of experimental data. Though the Morris-Lecar model is biologically meaningful (Izhikevich, 2004), it is difficult to make the assumption that the parameters are biophysically meaningful and measurable for any particular neuron in the respiratory CPG. The primary goal of this study is to replicate the behaviors of the original respiratory CPG, and the model seems to be too simple to reveal the inner details since a biological neuron is a complicated dynamic system with different types of ion channels and underlying neurotransmitters effects when coupled. Delay is proven to be effective for controlling the timing in artificial neural networks where the building block of single neuron models is relatively simple. By measuring the CPG's output pattern and sensory feedback, it is possible to set delay as a

function of the outside stimuli and thus provide the artificial CPG adaptability to the changing outside environment even when the inner mechanism remains unclear.

Numerical models are useful in scientific simulations to illustrate hidden mechanism, suggest new experiments and predict further outcomes. Artificial CPGs get attention in robotics benefiting from biological inspiration. Future work based on the artificial CPG model may involve 1) applying theories and methods of dynamical systems to the network, such as bifurcation theory to illustrate the inner details from a mathematical perspective; 2) adjustment to current neuron and synapse models to better approach the biological CPG.

Conclusion

In this study, we explored the electrophysiological fundamentals of action potential generation and the Hodgkin-Huxley mechanism of voltage-gated ion channels. We studied and analyzed the respiratory CPG in *Lymnaea stagnalis*, then replicated its output with the construction of an artificial CPG with ODE and DDE systems based on the Morris-Lecar model, which shows the feasibility of modelling CPG neural networks by existing neuron models with little or no experimental data. We hope this study will promote interest in computational neuroscience and many other interdisciplinary areas where computer science helps to better visualize the deep and great unknowns of this world.

Bibliography

Baars, B. J., & Gage, N. M. (2010). *Cognition, brain, and consciousness: Introduction to cognitive neuroscience*. Academic Press.

Bertram, R., Butte, M. J., Kiemel, T., & Sherman, A. (1995). Topological and phenomenological classification of bursting oscillations. *Bulletin of mathematical biology, 57(3)*, 413-439.

Borisyuk, A. (2015). Morris–Lecar Model. *Encyclopedia of Computational Neuroscience, (R. J. Dieter Jaeger, Ed.)* New York: Springer Science+Business Media.

Bungay, S. D., & Campbell, S. A. (2009). Modelling a Respiratory Central Pattern Generator Neuron in Lymnaea stagnalis. *Canadian applied mathematics quarterly, 17(2)*, 283-291.

Burkitt, A. N. (2006). A review of the integrate-and-fire neuron model: II. Inhomogeneous synaptic input and network properties. *Biological cybernetics, 95(2)*, 97-112.

Coombes, S., & Laing, C. (2009). Delays in activity-based neural networks. *Philosophical Transactions of the Royal Society A: Mathematical, Physical and Engineering Sciences, 367*(1891), 1117-1129.

Ditlevsen, S., & Greenwood, P. (2013). The Morris–Lecar neuron model embeds a leaky integrate-and-fire model. *Journal of Mathematical Biology, 67*(2), 239–259.

Gerstner, W., Kistler, W., Naud, R., & Paninski, L. (2014). *Neuronal Dynamics: From Single Neurons to Networks and Models of Cognition.* Cambridge University Press.

Graben, P. b., & Wright, J. (2011). From McCulloch–Pitts Neurons Toward Biology. *Bulletin of mathematical biology*, *73(2)*, 261-265.

González-Miranda, J. M. (2014). Pacemaker dynamics in the full Morris–Lecar model. *Communications in Nonlinear Science and Numerical Simulation, 19*(9), 3229-3241.

Hodgkin, A. L. (1948). The local electric changes associated with repetitive action in a non-medullated axon. *The Journal of Physiology, 107*(2), 165–181.

Hodgkin, A. L., & Huxley, A. F. (1952). A quantitative description of membrane current and its application to conduction and excitation in nerve. *The Journal of Physiology*, *117*(4)*,* 500–544.

Hopfield, J. J. (1982). Neural networks and physical systems with emergent collective computational abilities. *Proceedings of the National Academy of Sciences of the United States of America, 79*(8), 2554–2558.

Ijspeert, A. J. (2008). Central pattern generators for locomotion control in animals and robots: A review. *Auke, 21*(4), 642-653.

Izhikevich, E. M., Desai, N. S., Walcott, E. C., & Hoppensteadt, F. C. (2003). Bursts as a unit of neural information: selective communication via resonance. *Trends in neurosciences, 26*(3), 161-167.

Izhikevich, E. M. (2004). Which model to use for cortical spiking neurons? *IEEE Transactions on Neural Networks, 15*(5), 1063-070.

Izhikevich, Eugene M. (2006). Bursting. Scholarpedia. doi:10.4249/scholarpedia.1300

Izhikevich, Eugene M.; FitzHugh, Richard. (2006). FitzHugh-Nagumo model. Scholarpedia. doi:10.4249/scholarpedia.1349

Lecar, H. (2007). *Morris-Lecar model.* Scholarpedia. doi:10.4249/scholarpedia.1333

Lukowiak, K., & Syed, N. (1999). Learning, memory and a respiratory central pattern generator. *Comparative biochemistry and Physioloy. Part A, Molecular & integrative physiology, 124*(3), 265-274.

Lu, Q., Wang, Q., & Shi, X. (2009). *Delay Differential Equations - Recent Advances and New Directions, Ch10.* (B. Balachandran, T. Kalmár-Nagy, & D. E. Gilsinn, Eds.) New York, NY, USA: Springer.

Matveev, V., Bose, A., & Nadim, F. (2007). Capturing the bursting dynamics of a two-cell inhibitory network using a one-dimensional map. *Journal of Computational Neuroscience*, *23*(2), 169-187.

Nogaret, A., Zhao, L., Moraesb, D. J., & Patonb, J. F. (2013). Modulation of respiratory sinus arrhythmia in rats with central pattern generator hardware. *Jounal of Neuroscience Methods, 212* (1), 124–132.

Schwiening, C. J. (2012). A brief historical perspective: Hodgkin and Huxley. *The Journal of Physiology*, *590*(11) 2571–2575.

Syed, N. I., Bulloch, A. G., & Lukowiak, K. (1990). In vitro reconstruction of the respiratory central pattern generator of the mollusk Lymnaea. *Science, 250*(4978), 282-285.

Taylor, B. E., & Lukowiak, K. (2000). The respiratory central pattern generator of Lymnaea: a model, measured and malleable. *Respiration Physiology, 122*(2-3), 197-207.

Vavoulis, D. V., Straub, V. A., Kemenes, I., Kemenes,, G., Feng, J., & Benjamin, P. R. (2007). Dynamic control of a central pattern generator circuit: a computational model of the snail feeding network. *European Journal of Neuroscience, 25*(9), 2805–2818.

Vorontsov, D. D. (2002). Central Mechanisms that Control Respiration in the Pond Snail Lymnaea stagnalis: Is the VD4 Neuron Involved in Respiratory Rhythm Generation? *Doklady Biological Science, 386*(1), 436-439.

Yu, J., Tan, M., Chen, J., & Zhang, J. (2014, March). A Survey on CPG-Inspired Control Models and System Implementation. *IEEE Transactions on Neural Networks and Learning Systems, 25*(3), 441 - 456.

Appendix

Environment

Simulations of the neurons and neural network are done in Matlab R2013a

OS: Windows 7 professional, 64 bit

Hardware: RAM 16GB, CPU Intel Core i5-3470

ODE systems are solved by the built-in function ode45; DDE systems are solved by the built-in function dde23.

Source code

Computational model of HH type RPeD1 neuron and *f-I* curve

Files: b_and_tau_b.m, dydt_HH.m, h_and_tau_h.m, hp_and_tau_hp.m, mp_and_tau_mp.m, n_and_tau_n.m, q_and_tau_q.m define model with all the gating variables

1) b_and_tau_b.m gating variable b

```
function [b_inf]= b_and_tau_b(V)
```

```
aux=(V-(-69.1))/8.8;

b_inf=1./(1+exp(aux));

end
```

2) dydt_HH.m model definition

```
function dY=dydt_HH(t,Y,...

C,gbar_Na,gbar_Nap,gbar_Ca,gbar_KV,gbar_A,gbar_L,E_Na,E_Ca,E_K,E_L,Ifun)

V=Y(1);
m=Y(2);
h=Y(3);
mp=Y(4);
hp=Y(5);
r=Y(6);
s=Y(7);
n=Y(8);
q=Y(9);
b=Y(10);
tau_h=3.44;tau_hp=300;tau_r=10.5;tau_s=90;tau_b=200;

m_inf=1./(1 + exp((V-(-34.74))/(-9.32)));
tau_m=(6.98*exp(0.16*(V-(-34.74))/(-9.32)))*m_inf;
[h_inf]=h_and_tau_h(V);
[mp_inf, tau_mp]=mp_and_tau_mp(V);
[hp_inf]=hp_and_tau_hp(V);
r_inf=1/(1+exp((V-(-18.08))/(-7.2)));
s_inf=1/(1+exp((V-(-24.0))/8.7));
[n_inf, tau_n]=n_and_tau_n(V);
[q_inf, tau_q]=q_and_tau_q(V);
[b_inf]=b_and_tau_b(V);
I=Ifun;% uA/cm^2

dY=zeros(10,1);
dY(1)=(-1/C)*( gbar_Na*m^3*h*(V-E_Na) + gbar_Nap*mp^3*hp*(V-E_Na) +
gbar_Ca*r*s*(V-E_Ca) + gbar_KV*n^4*(V-E_K) + gbar_A*q^2*b*(V-E_K)...
              + gbar_L*(V-E_L) - I );
dY(2)=( m_inf-m )/tau_m;
dY(3)=( h_inf-h )/tau_h;
dY(4)=( mp_inf-mp )/tau_mp;
dY(5)=( hp_inf-hp )/tau_hp;
dY(6)=( r_inf-r )/tau_r;
dY(7)=(1/tau_s)*( s_inf-s );
dY(8)=(1/tau_n)*( n_inf-n );
dY(9)=(1/tau_q)*( q_inf-q );
dY(10)=(1/tau_b)*( b_inf-b );
end
```

3) h_and_tau_h gating variable h

```
function [h_inf, tau_h]= h_and_tau_h(V)
aux=(V-(-59.95))/9.4;
h_inf=1./(1+exp(aux));
```

```
tau_h=3.44; %ms
end
```

4) hp_and_tau_hp.m gating variable hp

```
function [hp_inf]= hp_and_tau_hp(V)
aux=(V-(-46))/7.43;
hp_inf=1./(1+exp(aux));
end
```

5) mp_and_tau_mp.m gating variable mp

```
function [mp_inf, tau_mp]= mp_and_tau_mp(V)
aux=(V-(-18))/(-16.4);
mp_inf=1./(1+exp(aux));
tau_mp=11.7+0.004*exp(V/(-7.6));
end
```

6) n_and_tau_n.m gating variable n

```
function [n_inf, tau_n]= n_and_tau_n(V)
aux=(V-(-42.5))/(-24.5);
n_inf=1./(1+exp(aux));
tau_n=62.56*exp(0.83*aux)*n_inf;
end
```

7) q_and_tau_q.m gating variable q

```
function [q_inf, tau_q]= q_and_tau_q(V)
aux=(V-(-62.3))/(-8.3);
q_inf=1./(1+exp(aux));
tau_q=16.1*exp(0.087*aux)*q_inf;
end
```

mainplot.m, main.m plot the spike trains of the RPeD1 neuron in figure 10 and the frequency – current curve in figure 8 respectively

8) mainplot.m

```
%Matlab code for plotting RPeD1 model.
%-----------------------------------------------
%F=farads
%V=mV
%A=amps
C=1.0;        %micro F/cm^2
gbar_Na=1.5; %(micro A/mV)/cm^2 i.e. mS/cm^
gbar_Nap=0.75;% mS/cm^2
gbar_Ca=0.15;% mS/cm^2
gbar_KV=0.6;    %(micro A/mV)/cm^2
gbar_A=0.03;
gbar_L=0.00075;    %(micro A/mV)/cm^2
E_Na=22;      %mV
E_Ca=80;      %mV
E_K=-70;      %mV
E_L=-12.2;      %mv
%V=Y(:,1);
%m=Y(:,2);
%h=Y(:,3);
%mp=Y(:,4);
%hp=Y(:,5);
```

```
%r=Y(:,6);
%s=Y(:,7);
%n=Y(:,8);
%q=Y(:,9);
%b=Y(:,10);


Y0=[-50,0,1,0,1,0,1,0,0,1];


t=0:1:12000;% milisecond ms
options=odeset('RelTol',1.e-6);
[T,
Y]=ode45(@dydt_HH,t,Y0,options,C,gbar_Na,gbar_Nap,gbar_Ca,gbar_KV,gbar_A,gbar
_L,E_Na,E_Ca,E_K,E_L,...
             0);

% Figure 1--Voltage vs Time
figure(1);
plot(T,Y(:,1)) % time course of V(t)
xlabel('Time (ms)')
ylabel('V (mV)')

% Figure 2--I (or V') vs V
figure(2);
vprime=diff(Y(:,1))./diff(T);
vcrec=(Y(1:(end-1),1)+Y(2:end,1))./2;
plot(vcrec,vprime)
% add an x-axis line at y=0 -- P.S.  the function was removed in R2014b
(which introduced the new HG2 graphics system)
hy = graph2d.constantline(0, 'Color',[.7 .7 .7]);
changedependvar(hy,'y');
xlabel('V')
ylabel('dv/dt')
```

9) main.m

```
%Plot frequency - current curve
C=1.0;        %micro F/cm^2
gbar_Na=1.5; %(micro A/mV)/cm^2 i.e. mS/cm^2
gbar_Nap=0.75;% mS/cm^2
gbar_Ca=0.15;% mS/cm^2
gbar_KV=0.6;    %(micro A/mV)/cm^2
gbar_A=0.03;
gbar_L=0.00075;    %(micro A/mV)/cm^2
E_Na=22;      %mV
E_Ca=80;      %mV
E_K=-70;      %mV
E_L=-12.2;      %mv



Y0=[-50,0,1,0,1,0,1,0,0,1];

% calculate frequency
```

```
grade=50;
spike=zeros(grade,1);
Ifun=zeros(grade,1);
for i=1:grade
    Ifun(i)= -.05+0.0025*i;
t=0:1:12000;% milisecond ms
options=odeset('RelTol',1.e-6);
[T,
Y]=ode45(@dydt_HH,t,Y0,options,C,gbar_Na,gbar_Nap,gbar_Ca,gbar_KV,gbar_A,gbar
_L,E_Na,E_Ca,E_K,E_L,...
             Ifun(i)); %graded input of current applied
 spike(i)=SpikeNum(Y(:,1),-30);
end


% Figure 1--Voltage vs Time
figure(1);
plot(T,Y(:,1)) % time course of V(t)
xlabel('Time (ms)')
ylabel('V (mV)')

%Figure 2 -- Mean spiking rate vs injected current
figure(2)
plot(Ifun,spike/20);
ylabel('frequency');
xlabel('current');
```

SpikeNum.m calculate the number of spikes for a simulation that facilitating calculating the frequency

10) SpikeNum.m

```
function NumSpikes = SpikeNum( v,threshold )
%SPIKENUM Calculate the Number of spikes in a certain input vector v, v
represents the voltage trace over time

%   if v[i]>threshold, count it as a spike

len=length(v);
NumSpikes=0;
for i=1:len-1
    if v(i) < threshold && v(i+1) >= threshold
        NumSpikes=NumSpikes+1;
    end

end
```

Computational model of Morris-Lecar based RPeD1 model and f-I curve

Files: MLODE.m, plotODEML.m, plotODEfI.m, SpikeNum.m

1) MLODE.m, model definition

```
% define ODEs of Morris-Lecar model
function dydt = MLODE(t, Y, zap)
```

```
VK=-84;      VL=-60;      VCa=120;
C=2;         phi=0.6667; V1=-12;
V2=18;       V3=-8;       V4=6.0;
gCa=4.0;     gK=8.0;      gL=2.0;

Cinv=1.0/C;
I=zap;

minf=0.5*(1+tanh((Y(1)-V1)/V2));
winf=0.5*(1+tanh((Y(1)-V3)/V4));
kW=cosh((Y(1)-V3)/(2*V4));

dydt=[Cinv*(-gCa*minf*(Y(1)-VCa) - gK*Y(2)*(Y(1)-VK) - gL*(Y(1)-VL)  + I);
phi * (winf - Y(2)) * kW];
```

2) plotODEfI.m, plot frequency-current curve, figure 8

```
ICS(1,1:2) = [-23.1  0.00104 ];
ICS(2,1:2) = [-38.7  0.00848 ];
ICS(3,1:2) = [-58.3  0.425 ];
ICS(4,1:2) = [-56    0  ];
ICS(5,1:2) = [-58.1  0.591  ];

T=1200;

%set initial conditions
%IC=[-15  0.0149]
IC=ICS(5,:)
options = [];
options = odeset(options,'RelTol',1e-4);
% calculate frequency
grade=50;
spike=zeros(grade,1);
Ifun=zeros(grade,1);
for i=1:grade
Ifun(i)= 0+0.5*i;


[t,y] = ode45(@MLODE, [0 T], IC,options, Ifun(i));
%plot(t,y(:,1));
 spike(i)=SpikeNum(y(:,1),-30);
end

%Figure 2 -- Mean spiking rate vs injected current
figure(2)
plot(Ifun,spike/20);
ylabel('frequency');
xlabel('current');
```

3) plotODEML.m, plot spike trains, figure 11

```
ICS(1,1:2) = [-23.1  0.00104 ];
ICS(2,1:2) = [-38.7  0.00848 ];
ICS(3,1:2) = [-58.3  0.425 ];
ICS(4,1:2) = [-56    0  ];
ICS(5,1:2) = [-58.1  0.591  ];

T=300;

%set initial conditions
IC=ICS(5,:)
options = [];
options = odeset(options,'RelTol',1e-4);

Iapp=14;

[t,y] = ode45(@MLODE, [0 T], IC,options, Iapp);
plot(t,y(:,1));
xlabel('Time(ms)')
ylabel('V(mv)')
```

Computational model of the artificial CPG as an ODE system

Files: burstODE.m, plotODE.m

1) burstODE.m, model definition

```
% An artificial CPG modeled as a set of ODEs
% 3 neurons neural network: HCO + ML
% A half-center oscillator and a pacemaker (based on Morris Lecar model)

% Parameters of HCO adapted from the paper below
% "Capturing the bursting dynamics of a two-cell inhibitory network using a
one-dimensional map"


function dydt = burstODE(t, Y)

% Basic parameters of Neuron1 and Neuron2
gbarsyn = 1.1;
gT = 1.38; Vh = -52;
tauSyn = 1; tgamma = 0.2;
tlo = 100; thi = 20;
vthresh = -3;

VK=-84;     VL=-60;     VCa=120;
C=2;        phi=0.6667; V1=-12;
V2=18;      V3=-8;      V4=6.0;
gCa=4.0;    gK=8.0;
gL=3;
Cinv=1.0/C; einh=-80;
vax=Vh;     vix=Vh;
slope=4;
```

```
zap=14;

% Additional parameters of Neuron0
gL0=2.3;
zap0=20;% injected current in Neuron0
einh_ex=-20;
eexc=-20;
slope0=slope;
%vthresh0
vthresh0=15;
tgamma0=tgamma;
%tauSyn0
tauSyn0=5;
%gbarsyn0
gbarsyn0=1;

%Neuron1
minf=0.5*(1+tanh((Y(1)-V1)/V2));
winf=0.5*(1+tanh((Y(1)-V3)/V4));
kW=cosh((Y(1)-V3)/(2*V4));
%Neuron2
minf1=0.5*(1+tanh((Y(2)-V1)/V2));
winf1=0.5*(1+tanh((Y(2)-V3)/V4));
kW1=cosh( (Y(2) - V3) / (2 * V4) );

ax=0.5*(1+tanh(slope*(Y(1)-vax)));% For IT of N1

ax1=0.5*(1+tanh(slope*(Y(2)-vax)));% for IT of N2

%Neuron0
minf0=0.5*(1+tanh((Y(9)-V1)/V2));
winf0=0.5*(1+tanh((Y(9)-V3)/V4));
kW0=cosh((Y(9)-V3)/(2*V4));

dydt=[Cinv*(-gCa*minf*(Y(1)-VCa) - gK*Y(3)*(Y(1)-VK) - gL*(Y(1)-VL) -
gT*ax*Y(5)*(Y(1)-VCa) - gbarsyn*Y(8)*(Y(1)-einh) - gbarsyn*Y(11)*(Y(1)-
einh_ex) + zap);
Cinv * (-gCa*minf1*(Y(2)-VCa) - gK*Y(4)*(Y(2)-VK) - gL*(Y(2)-VL) -
gT*ax1*Y(6)*(Y(2)-VCa) - gbarsyn*Y(7)*(Y(2)-einh) - gbarsyn*Y(13)*(Y(2)-
einh)+ zap);
phi * (winf - Y(3)) * kW;
phi * (winf1 - Y(4)) * kW1;
(1-Y(5))*0.5*(1 + tanh(slope*(vix-Y(1))))/tlo - Y(5)*0.5*(1 +
tanh(slope*(Y(1)-vix)))/thi;
(1-Y(6))*0.5*(1 + tanh(slope*(vix-Y(2))))/tlo - Y(6)*0.5*(1 +
tanh(slope*(Y(2)-vix)))/thi;
(1-Y(7))*0.5*(1 + tanh(slope*(Y(1)-vthresh)))/tgamma - Y(7)*0.5*(1 +
tanh(slope*(vthresh-Y(1))))/tauSyn;
(1-Y(8))*0.5*(1 + tanh(slope*(Y(2)-vthresh)))/tgamma - Y(8)*0.5*(1 +
tanh(slope*(vthresh-Y(2))))/tauSyn;
Cinv*(-gCa*minf0*(Y(9)-VCa) - gK*Y(10)*(Y(9)-VK) - gL0*(Y(9)-VL)  -
gbarsyn0*Y(12)*(Y(9)-eexc) - gbarsyn0*Y(14)*(Y(9)-einh) + zap0);
phi * (winf0 - Y(10)) * kW0;
(1-Y(11))*0.5*(1 + tanh(slope0*(Y(9)-vthresh0)))/tgamma0 - Y(11)*0.5*(1 +
tanh(slope0*(vthresh0-Y(9))))/tauSyn0;
```

```
(1-Y(12))*0.5*(1 + tanh(slope*(Y(1)-vthresh)))/tgamma - Y(12)*0.5*(1 +
tanh(slope*(vthresh-Y(1))))/tauSyn;
(1-Y(13))*0.5*(1 + tanh(slope0*(Y(9)-vthresh0)))/tgamma0 - Y(13)*0.5*(1 +
tanh(slope0*(vthresh0-Y(9))))/tauSyn0
(1-Y(14))*0.5*(1 + tanh(slope*(Y(2)-vthresh)))/tgamma - Y(14)*0.5*(1 +
tanh(slope*(vthresh-Y(2))))/tauSyn];
```

2) plotODE.m, Figure 15-19

```
% Plot the output of artificial CPG
T=800;
IC = [-58.3 -34.1 0       0.425  0.0951 0.126  0     0.647, 20 0 0 0.015 0
0.54 ];
options = [];
options = odeset(options,'RelTol',1e-4);


[t,y] = ode23t(@burstODE, [0 T], IC, options);

% Voltage vs Time

figure(1)

plot(t,y(:,9),'g',t,y(:,1),'r',t,y(:,2),'b');
legend('v0','v1','v2');
xlabel('Time(ms)')
ylabel('V(ms)')

figure(2)

subplot(3,1,1)
plot(t, y(:,9))
xlabel('Time(ms)')
ylabel('v0')

subplot(3,1,2)
plot(t, y(:,1))
xlabel('Time(ms)')
ylabel('v1')

subplot(3,1,3)
plot(t, y(:,2))
xlabel('Time(ms)')
ylabel('v2')

% Other variables vs time

figure(3)
subplot(3,1,1)
plot(t,y(:,3))
xlabel('Time(ms)')
ylabel('w1')

subplot(3,1,2)
```

```
plot(t,y(:,4))
xlabel('Time(ms)')
ylabel('w2')

subplot(3,1,3)
plot(t,y(:,10))
xlabel('Time(ms)')
ylabel('w0')

figure(4)
subplot(2,1,1)
plot(t,y(:,5))
xlabel('Time(ms)')
ylabel('h1')

subplot(2,1,2)
plot(t,y(:,6))
xlabel('Time(ms)')
ylabel('h2')

figure(5)
subplot(2,1,1)
plot(t,y(:,7))
xlabel('Time(ms)')
ylabel('s12')

subplot(2,1,2)
plot(t,y(:,8))
xlabel('Time(ms)')
ylabel('s21')

figure(6)
subplot(2,1,1)
plot(t,y(:,11))
xlabel('Time(ms)')
ylabel('s01')

subplot(2,1,2)
plot(t,y(:,12))
xlabel('Time(ms)')
ylabel('s10')

figure(7)
subplot(2,1,1)
plot(t,y(:,13))
xlabel('Time(ms)')
ylabel('s02')

subplot(2,1,2)
plot(t,y(:,14))
xlabel('Time(ms)')
ylabel('s20')
```

Computational model of the artificial CPG as an DDE system

Files: burstDE.m, plotDE.m

1) burstDE.m, model definition

```
function dydt = burstDE(t, Y, Z)

Params = [1.1 1.38 -52 1 0.2 100 20 -3];
ylag1= Z(:,1);
ylag2= Z(:,2);

gbarsyn = Params(1);
gtbar = Params(2); Vh = Params(3);
tauSyn = Params(4); tgamma = Params(5);
tlo = Params(6); thi = Params(7);
vthresh = Params(8);

VK=-84;     VL=-60;     VCa=120;
C=2;        phi=0.6667; V1=-12;
V2=18;      V3=-8;      V4=6.0;
gCa=4.0;    gK=8.0;
gL=3;
Cinv=1.0/C; einh=-80;
vax=Vh;     vix=Vh;
slope=4;
zap=14;

% Additional parameters of Neuron0

gL0=2.3;

zap0=20;% injected current in Neuron0
einh_ex=-20;
eexc=-20;
slope0=slope;

vthresh0=20;
tgamma0=tgamma;

tauSyn0=15;

gbarsyn0=1;

%Neuron1
minf=0.5*(1+tanh((Y(1)-V1)/V2));
winf=0.5*(1+tanh((Y(1)-V3)/V4));
kW=cosh((Y(1)-V3)/(2*V4));
%Neuron2
minf1=0.5*(1+tanh((Y(2)-V1)/V2));
winf1=0.5*(1+tanh((Y(2)-V3)/V4));
kW1=cosh( (Y(2) - V3) / (2 * V4) );

ax=0.5*(1+tanh(slope*(Y(1)-vax)));% For IT of N1
```

```
ax1=0.5*(1+tanh(slope*(Y(2)-vax)));% for IT of N2

%Neuron0
minf0=0.5*(1+tanh((Y(9)-V1)/V2));
winf0=0.5*(1+tanh((Y(9)-V3)/V4));
kW0=cosh((Y(9)-V3)/(2*V4));

dydt=[Cinv*(-gCa*minf*(Y(1)-VCa) - gK*Y(3)*(Y(1)-VK) - gL*(Y(1)-VL) -
gtbar*ax*Y(5)*(Y(1)-VCa) - gbarsyn*Y(8)*(Y(1)-einh) - gbarsyn*Y(11)*(Y(1)-
einh_ex) + zap);
Cinv * (-gCa*minf1*(Y(2)-VCa) - gK*Y(4)*(Y(2)-VK) - gL*(Y(2)-VL) -
gtbar*ax1*Y(6)*(Y(2)-VCa) - gbarsyn*Y(7)*(Y(2)-einh) - gbarsyn*Y(13)*(Y(2)-
einh)+ zap);
phi * (winf - Y(3)) * kW;
phi * (winf1 - Y(4)) * kW1;
(1-Y(5))*0.5*(1 + tanh(slope*(vix-Y(1))))/tlo - Y(5)*0.5*(1 +
tanh(slope*(Y(1)-vix)))/thi;
(1-Y(6))*0.5*(1 + tanh(slope*(vix-Y(2))))/tlo - Y(6)*0.5*(1 +
tanh(slope*(Y(2)-vix)))/thi;
(1-Y(7))*0.5*(1 + tanh(slope*(ylag1(1)-vthresh)))/tgamma - Y(7)*0.5*(1 +
tanh(slope*(vthresh-ylag1(1))))/tauSyn;
(1-Y(8))*0.5*(1 + tanh(slope*(ylag2(2)-vthresh)))/tgamma - Y(8)*0.5*(1 +
tanh(slope*(vthresh-ylag2(2))))/tauSyn;
Cinv*(-gCa*minf0*(Y(9)-VCa) - gK*Y(10)*(Y(9)-VK) - gL0*(Y(9)-VL)  -
gbarsyn0*Y(12)*(Y(9)-eexc) - gbarsyn0*Y(14)*(Y(9)-einh) + zap0);
phi * (winf0 - Y(10)) * kW0;
(1-Y(11))*0.5*(1 + tanh(slope0*(Y(9)-vthresh0)))/tgamma0 - Y(11)*0.5*(1 +
tanh(slope0*(vthresh0-Y(9))))/tauSyn0;
(1-Y(12))*0.5*(1 + tanh(slope*(Y(1)-vthresh)))/tgamma - Y(12)*0.5*(1 +
tanh(slope*(vthresh-Y(1))))/tauSyn;
(1-Y(13))*0.5*(1 + tanh(slope0*(Y(9)-vthresh0)))/tgamma0 - Y(13)*0.5*(1 +
tanh(slope0*(vthresh0-Y(9))))/tauSyn0;
(1-Y(14))*0.5*(1 + tanh(slope*(Y(2)-vthresh)))/tgamma - Y(14)*0.5*(1 +
tanh(slope*(vthresh-Y(2))))/tauSyn];
```

2) plotDE.m Figure 20-21

```
T=1500;
IC = [-58.3 -34.1 0  0.425  0.0951 0.126  0   0.647, 20 0 0 0.015 0 0.54 ];

% 2 delays
delay=[75,150];
sol = dde23(@burstDE,delay,IC,[0, T]);

% Voltage vs Time
figure(1)
plot(sol.x,sol.y(9,:),'g', sol.x,sol.y(1,:),'r',sol.x,sol.y(2,:),'b');
legend('v0','v1','v2');
xlabel('Time(ms)')
ylabel('V(mv)')

figure(2)
subplot(3,1,1)
```

```
plot(sol.x, sol.y(9,:))
xlabel('Time(ms)')
ylabel('v0')

subplot(3,1,2)
plot(sol.x, sol.y(1,:))
xlabel('Time(ms)')
ylabel('v1')

subplot(3,1,3)
plot(sol.x, sol.y(2,:))
xlabel('Time(ms)')
ylabel('v2')


% Other variables vs time
figure(3)
subplot(3,1,1)
plot(sol.x,sol.y(3,:))
xlabel('Time(ms)')
ylabel('w1')

subplot(3,1,2)
plot(sol.x,sol.y(4,:))
xlabel('Time(ms)')
ylabel('w2')

subplot(3,1,3)
plot(sol.x,sol.y(10,:))
xlabel('Time(ms)')
ylabel('w0')

figure(4)
subplot(2,1,1)
plot(sol.x,sol.y(5,:))
xlabel('Time(ms)')
ylabel('h1')

subplot(2,1,2)
plot(sol.x,sol.y(6,:))
xlabel('Time(ms)')
ylabel('h2')

figure(5)
subplot(2,1,1)
plot(sol.x,sol.y(7,:))
xlabel('Time(ms)')
ylabel('s12')

subplot(2,1,2)
plot(sol.x,sol.y(8,:))
xlabel('Time(ms)')
ylabel('s21')

figure(6)
```

```
subplot(2,1,1)
plot(sol.x,sol.y(11,:))
xlabel('t')
ylabel('s01')

subplot(2,1,2)
plot(sol.x,sol.y(12,:))
xlabel('Time(ms)')
ylabel('s10')

figure(7)
subplot(2,1,1)
plot(sol.x,sol.y(13,:))
xlabel('Time(ms)')
ylabel('s02')

subplot(2,1,2)
plot(sol.x,sol.y(14,:))
xlabel('Time(ms)')
ylabel('s20')
```